

POLITECNICO DI TORINO

Corso di Laurea Magistrale
in Ingegneria Energetica e Nucleare

Tesi di Laurea Magistrale

**Numerical model for the analysis
of thermal transients in district
heating networks**



Relatori

Prof. Vittorio Verda
Dott. Elisa Guelpa

Candidata

Martina Capone

A.A. 2017/2018

Abstract

The aim of this work is to propose a model to evaluate the thermo-fluid dynamic behaviour of district heating networks, with special care on the prediction of thermal transients. An accurate description of the temperature evolution within the plant is needed to better design new systems or expanding the existing ones, in order to optimize the energy release from the plant to the network and avoid thermal losses, so that the pollutant emissions are reduced and the cost of heating is kept sufficiently low.

A brief overview of the existing models is detailed, especially for what concerns the hydraulic part. Moreover, the main weaknesses of the typically used thermal models, that are mainly based on the Upwind Differencing Scheme, are described. Different strategies to avoid the effect of the artificial diffusivity are analysed.

A chapter is also dedicated to the study of the effects of the application of adaptive moving mesh methods to a one-dimensional model problem completely dominated by advection.

Finally, the model is developed taking advantage of the Quadratic Upstream Interpolation for Convective Kinematics (QUICK), and an example of application is proposed to test it.

Acknowledgements

I would like to sincerely acknowledge my supervisors, Prof. Vittorio Verda and Dott. Elisa Guelpa, for their support and their insightful suggestions for the realisation of this thesis.

I extend my thanks to all the people that I met during this exciting journey at Politecnico di Torino, to my old friends and to the ones that I met during these years, for all the moments we shared.

Special thanks goes to Davide, for being always by my side.

Finally, I want to express my gratitude to my parents, who gave me this opportunity and always encouraged me. Without them I wouldn't have made it this far.

Contents

List of Figures	3
1 Introduction	6
2 Thermo-fluid dynamic model of district heating networks	8
2.1 The graph approach	9
2.2 The fluid-dynamic problem	10
2.3 The SIMPLE algorithm	14
3 The thermal problem	18
3.1 The central differencing scheme	22
3.1.1 Steady-state advection-diffusion model problem	22
3.1.2 Conservativeness and boundedness	25
3.2 The upwind scheme	28
3.2.1 Steady-state advection-diffusion model problem	28
3.2.2 Transient pure advection model problem	30
4 The problem of numerical diffusion	34
4.1 Method of characteristics	35
4.2 TRNSYS Type31 Model	36

4.3	Quadratic Upstream Interpolation for Convective Kinematics (QUICK)	37
4.3.1	Transient pure-advection model problem	39
5	Adaptive moving mesh methods	43
5.1	Transient pure advection model problem	45
5.1.1	Upwind differencing scheme	47
5.1.2	QUICK	48
6	Description of the thermal model	53
6.1	Approximation of wall values with QUICK	55
6.2	Approximation of wall values with USD	57
6.3	Example of application	59
7	Conclusions	67
	Bibliography	69

List of Figures

2.1	Schematic of the SIMPLE algorithm [9].	17
3.1	Schematic of the control volume of a node [9].	20
3.2	A control volume around node P . Modified from [17].	23
3.3	Numerical CDS solution and exact solution of the one-dimensional steady-state advection-diffusion problem with three different Peclet numbers.	26
3.4	Example of consistent specification of diffusive fluxes [17].	27
3.5	Numerical UDS solution of the one-dimensional transient pure advection problem at different times, solved using four grids of different quality.	31
3.6	Numerical UDS solution of four different grids and exact solution of the one-dimensional transient pure advection problem at $t = 0.5 s$	32
4.1	Solution of the transient pure advection problem at different times, obtained using the method of characteristics, $N = 100$	36
4.2	Lagrangian coordinate system for one-dimensional system [10].	36
4.3	Quadratic upstream interpolation for T_e , adapted from [19].	38
4.4	Quadratic upstream interpolation for T_w , adapted from [19].	39

4.5	Numerical QUICK solution of the one-dimensional transient pure advection problem at different times, solved using four grids of different quality.	40
4.6	Numerical QUICK solution of the one-dimensional transient pure advection problem at $t = 0.5 s$ for $N = 10$, $N = 100$, $N = 1000$ and $N = 10000$	40
4.7	Numerical QUICK and UDS solutions compared to the exact one at $t = 0.5 s$ and with $N = 100$	41
4.8	Numerical QUICK ($N = 100$) and UDS ($N = 1000$) solutions compared to the exact one at $t = 0.5 s$	41
5.1	On the left, numerical UDS solution on a non-uniform adaptive grid of the one-dimensional transient pure advection problem every $0.1 s$. On the right, the centroids of the corresponding adaptive moving mesh.	47
5.2	Numerical UDS solution of the one-dimensional transient pure advection problem on an adaptive grid and on a uniform one, at $t = 0.5 s$	48
5.3	On the left, numerical QUICK solution on a non-uniform adaptive grid of the one-dimensional transient pure advection problem every $0.1 s$. On the right, the centroids of the corresponding adaptive moving mesh.	51
5.4	Numerical QUICK solution of the one-dimensional transient pure advection problem on an adaptive grid and on a uniform one, at $t = 0.5 s$	51
6.1	Example of the upwind scheme for a node [11].	58
6.2	Schematic of the district heating network [11].	60

6.3	Temperature distribution at $t = 1800 s$ in the <i>real</i> nodes, obtained inserting a <i>fictitious</i> node every $10 m$ and using a time step of $1 s$. . .	63
6.4	Temperature distribution at $t = 3600 s$ in the <i>real</i> nodes, obtained inserting a <i>fictitious</i> node every $10 m$ and using a time step of $1 s$. . .	63
6.5	Temperature evolution of node 14, obtained inserting a <i>fictitious</i> node every $10 m$ and using a time step of $1 s$	64
6.6	Temperature distribution at $t = 1800 s$ in the <i>real</i> nodes, obtained inserting a <i>fictitious</i> node every $5 m$ and using a time step of $1 s$. . .	65
6.7	Temperature distribution at $t = 3600 s$ in the <i>real</i> nodes, obtained inserting a <i>fictitious</i> node every $5 m$ and using a time step of $1 s$. . .	65
6.8	Temperature evolution of node 14, obtained inserting a <i>fictitious</i> node every $5 m$ and using a time step of $1 s$	66

Chapter 1

Introduction

District energy systems can be described as methods by which thermal energy from a central source is distributed to residential, commercial and industrial consumers for use in space heating, cooling, water heating and process heating [1].

District heating networks appeared in Europe since the 14th century [2], and they have been developed since 1950 [3]. Nowadays, there are more than 5000 district heating systems in Europe, covering more than 10% of total European heat demand [4]. Market penetration is unevenly distributed: it is close to zero in some countries, while it reaches more than 70% of heat market in others.

District Heating and Cooling represent the most suitable solution for providing heat and cold to urban users, since their benefits are most apparent in areas with high density energy demand [4]. Apart from urban environments, also energy demands from industry and intensive agriculture are suitable to be satisfied by the use of district heating. In these sectors an additional benefit is given by the fact that CO_2 emissions for industrial processes and green-houses can be captured and transported.

Overall, district heating and cooling systems provide a reliable and competitive

energy service, which is able to satisfy user demands and to reduce primary energy consumptions, responding to the main European energy policy objectives. Indeed, the fundamental idea of district heating is to use local fuel or heat resources that would otherwise be wasted [5]. In particular, district heating uses excess heat resources from combined heat and power (CHP) plants, waste-to-energy plants (WtE) and industrial process, and in the last years, it introduced renewable sources like geothermal wells, solar collectors and biomass fuels [6].

Thanks to the large number of benefits that district heating technology can boast, such as higher security of supply, lower costs and lower carbon dioxide and pollutant emissions, the future prospects for district heating and cooling technology should be promising [6].

Due to the large investment costs required by the extension of existing networks and construction of newest small ones, there is a great interest in simulations and solutions which can lead to the reduction of distribution losses, limiting the overuse of peak generators and optimizing the use of centralized and decentralized storage capacities [7]. In this sense, the analysis of the thermal transients in the network assumes a key role.

Some models have been proposed to solve the thermo-fluid dynamic problem of large district heating networks [8] [9]. This work proposes a numerical thermo-fluid dynamic model of district heating-networks that, differently from the models typically used, pays particular attention to the prediction of temperature behaviour, and tries to avoid the problems, like the introduction of artificial diffusion, that usually come out when differential equations are solved by means of numerical schemes.

Chapter 2

Thermo-fluid dynamic model of district heating networks

The analysis of a district heating network usually involves the evaluation of mass flow rates flowing in the system and the prediction of pressure and temperature evolution in some crucial points. Indeed, the control of these parameters is a key challenge to reduce heat losses and to minimize the heat cost while ensuring the user comfort in buildings [10].

One way to evaluate these quantities is to equip the network with proper instrumentation to measure temperatures and mass flow rates at numerous locations. This solution is typically too expensive due to the large cost of sensors and to the intrinsically intrusive nature of this method. Therefore, an appropriate model is needed to forecast the thermo-fluid dynamic behaviour of the network. Moreover, modelling the network leads to the possibility to analyse different conditions with respect to the operating ones and various layout, evaluating the effects of these changes without the need to carry out expensive and not always reliable experimental tests.

The model is based on the conservation equations. In particular, velocity and pressure in a flow system are governed by the continuity and the momentum equation [11]:

$$\frac{\partial \rho}{\partial t} + \nabla \cdot \rho \mathbf{v} = 0 \quad (2.1)$$

$$\rho \frac{D\mathbf{v}}{Dt} = -\nabla p - \nabla \cdot \boldsymbol{\tau} + \mathbf{F} , \quad (2.2)$$

where $\nabla \cdot \boldsymbol{\tau}$ represents the net force due to viscous stress and \mathbf{F} is a momentum source term that also includes the gravity term $\rho \mathbf{g}$. Then, energy conservation equation reads:

$$\frac{\partial(\rho c_p T)}{\partial t} + \nabla \cdot (\rho c_p \mathbf{v} T) = \nabla \cdot k \nabla T + \varphi_s . \quad (2.3)$$

The model used is a *pseudo-dynamic* model [12]: only heat transfer is simulated dynamically, while for hydraulic phenomena the unsteady term is not considered. The reason behind this choice is that fluid-dynamic perturbations are quickly transferred to the whole network, in a period of time of few seconds, smaller than the time step adopted for calculations. Oppositely, temperature perturbations travel at the fluid velocity, which is typically of the order of few meters per second, and their effects are transferred to the DHN slowly.

2.1 The graph approach

The model adopted to simulate the problem is one-dimensional. The complex structure of a district heating network, made of components (pipes) that are connected to each other through junctions, is described by means of the graph theory [13]. A graph is a representation of a set of connected objects: each connection involves a pair of objects (nodes), but each object can be connected to multiple other objects

through multiple links (branches). For a district heating network, nodes usually corresponds to junctions, and branches, that are elements bounded by two nodes, to components such as duct, channel, etc.

A flow network is described by means of the interconnections between nodes and branches. These interconnections represent the network topology, and they are described by means of the incidence matrix \mathbf{A} , which has as many rows as the number of nodes and as many columns as the number of branches. A general element A_{ij} is equal to 1 if the i -th node is the inlet node of the j -th branch, or it is equal to -1 if the i -th node is the outlet node of the j -th branch. Otherwise, the i -th node and the j -th branch are not related and the element is equal to 0.

2.2 The fluid-dynamic problem

In the case of a one-dimensional description of the system, equations (2.1) and (2.2) simplify to:

$$\frac{\partial \rho}{\partial t} + \frac{\partial(\rho v_1)}{\partial x_1} = 0 \quad (2.4)$$

$$\rho \frac{\partial v_1}{\partial t} + \rho v_1 \frac{\partial v_1}{\partial x_1} = -\frac{\partial p}{\partial x_1} - F_{FRICT} + F_1, \quad (2.5)$$

where F_{FRICT} takes into account the viscous forces, replacing the term $(\nabla \cdot \boldsymbol{\tau})_1$ that loses significance in the case of one-dimensional formulation, and F_1 represents the source term and accounts also for the effect of local fluid dynamic resistance due to valves or junctions and the effects of pressure rise due to pumps or fans. According to [11], it can be expressed as:

$$F_1 = \rho g_{x_1} - F_{LOCAL} + F_{PUMP}. \quad (2.6)$$

Continuity equation (2.4) can be integrated over a control volume including the junction node and half of each branch entering or exiting it. After this integration, one obtains:

$$\frac{dM}{dt} + \sum_{j=1}^{NB} \rho_j v_{1,j} S_j = 0 , \quad (2.7)$$

where M is the mass of fluid in the control volume, NB is the total number of branches entering or exiting the control volume and S_j represents the section of the j -th branch. Equation 2.7 must be modified in order to take into account a possible extraction or injection of fluid from a junction to the external ambient. Then, considering also that $G_j = \rho_j v_{1,j} S_j$, it becomes:

$$\frac{dM}{dt} + \sum_{j=1}^{NB} G_j + G_{ext} = 0 , \quad (2.8)$$

and, remembering the aforementioned steady-state conditions for the fluid dynamic problem:

$$\sum_{j=1}^{NB} G_j + G_{ext} = 0 . \quad (2.9)$$

Using the incidence matrix \mathbf{A} , it is possible to apply the continuity equation to all the nodes of the network, obtaining:

$$\mathbf{A} \cdot \mathbf{G} + \mathbf{G}_{ext} = \mathbf{0} , \quad (2.10)$$

where \mathbf{G} is a column vector containing the mass flow rates in the branches and \mathbf{G}_{ext} the vector that contains the mass flow rates injected or extracted in the nodes from the external environment.

Momentum equation (2.5) is instead integrated over a control volume which includes

a branch and the two delimiting nodes. This integration brings to:

$$\begin{aligned} \rho \frac{\partial v_1}{\partial t} V + \rho \frac{v_{1,out}^2 - v_{1,in}^2}{2} S = & (p_{in} - p_{out}) S - \rho g (z_{out} - z_{in}) S \\ & - \Delta P_{FRICT} S - \Delta P_{LOCAL} S + \Delta P_{PUMP} S, \end{aligned} \quad (2.11)$$

where $V = SL$ is the volume of the considered control volume, S its cross section and L its length. Defining the total pressure as $P := p + \rho \frac{v^2}{2} + \rho g z$, equation (2.11) can be rewritten as:

$$\rho \frac{\partial v_1}{\partial t} L + (P_{out} - P_{in}) = -\Delta P_{FRICT} - \Delta P_{LOCAL} + \Delta P_{PUMP}. \quad (2.12)$$

The terms ΔP_{FRICT} and ΔP_{LOCAL} can be formulated according to the expressions given by [14]:

$$\Delta P_{FRICT} = f \frac{L}{D} \frac{1}{2} \rho v_1^2, \quad (2.13)$$

$$\Delta P_{LOCAL} = \sum_k \beta_k \frac{1}{2} \rho v_1^2, \quad (2.14)$$

where f is the friction factor, β_k is the localized pressure drop coefficient and the summation refers to the different local losses that may occur in a duct. The values of these coefficients can be found in literature.

Substituting (2.13) and (2.14) in equation (2.12), and assuming, as previously explained, the fluid-dynamic problem a steady-state, it is possible to obtain:

$$P_{in} - P_{out} = \frac{1}{2} \rho v_1^2 \left(f \frac{L}{D} + \sum_k \beta_k \right) - \Delta P_{PUMP}, \quad (2.15)$$

which is equivalent to:

$$P_{in} - P_{out} = \frac{1}{2} \frac{G^2}{\rho S^2} \left(f \frac{L}{D} + \sum_k \beta_k \right) - \Delta P_{PUMP}. \quad (2.16)$$

As done in the case of continuity, equation (2.16) can be extended to the whole network using the matrix formulation:

$$\mathbf{A}^T \cdot \mathbf{P} = \mathbf{R} \cdot \mathbf{G} - \mathbf{t}, \quad (2.17)$$

where \mathbf{A}^T is the transpose of the incidence matrix, \mathbf{P} is a vector containing the pressures at the nodes, \mathbf{G} is the vector containing the values of mass flow rates in the branches, \mathbf{t} is a vector that contains the terms accounting for the pressure increases due to pumps, and \mathbf{R} is a diagonal matrix that contains the terms:

$$R_j = \frac{1}{2} \frac{G_j}{\rho S_j^2} \left(f_j \frac{L_j}{D_j} + \sum_k \beta_{k,j} \right). \quad (2.18)$$

Isolating \mathbf{G} , one gets:

$$\mathbf{G} = \mathbf{Y} \cdot \mathbf{A}^T \cdot \mathbf{P} + \mathbf{Y} \cdot \mathbf{t}, \quad (2.19)$$

being $\mathbf{Y} = \mathbf{R}^{-1}$, which represents the fluid dynamic conductance. Proper boundary conditions need to be applied on equation (2.19): typically the pressure is set on the node representing the pressurization system [9]. Moreover, the boundary conditions concerning mass flow rates entering or exiting the network must be imposed on \mathbf{G}_{ext} .

2.3 The SIMPLE algorithm

Due to the fact that the matrix \mathbf{Y} contains itself a dependence on the mass flow rates, the system of equations is non-linear. This non-linearity, together with the strict coupling between mass (2.10) and momentum (2.19) equations, brings to the need of an iterative algorithm to solve the problem. According to [9], the SIMPLE (semi-implicit method for pressure linked equation) algorithm [15] can be efficiently applied to this scope. This algorithm is based on a guess and correction method: a vector \mathbf{P}' is first guessed and then corrected during the iterations with the mass flow rate resulting from (2.19). Once guessed \mathbf{P}' , another initial guess is made for \mathbf{G}'_0 . This is needed to build \mathbf{Y}' , in order to be able to obtain \mathbf{G}' :

$$\mathbf{G}' = \mathbf{Y}' \cdot \mathbf{A}^T \cdot \mathbf{P}' + \mathbf{Y}' \cdot \mathbf{t} . \quad (2.20)$$

Equation (2.20) is non-linear, and it is solved using the fixed point algorithm [16]. The guessed values of pressure and mass flow rates differ from the correct values. Therefore, it is possible to define a correction, both for mass flow \mathbf{G}_{corr} and for pressure \mathbf{P}_{corr} , such that:

$$\mathbf{P} = \mathbf{P}' + \mathbf{P}_{\text{corr}} , \quad (2.21)$$

$$\mathbf{G} = \mathbf{G}' + \mathbf{G}_{\text{corr}} . \quad (2.22)$$

Combining together equations (2.19) and (2.20), one gets:

$$\mathbf{G} - \mathbf{G}' = \mathbf{Y} \cdot \mathbf{A}^T \cdot \mathbf{P} - \mathbf{Y}' \cdot \mathbf{A}^T \cdot \mathbf{P}' + (\mathbf{Y} - \mathbf{Y}') \cdot \mathbf{t} . \quad (2.23)$$

Then, taking as assumption $\mathbf{Y}' = \mathbf{Y}$ and substituting in (2.23) the expressions (2.21) and (2.22), it is possible to obtain:

$$\mathbf{G}_{\text{corr}} = \mathbf{Y} \cdot \mathbf{A}^T \cdot \mathbf{P}_{\text{corr}} . \quad (2.24)$$

Moreover, expression (2.22) can be substituted into the conservation of mass expressed by (2.10), getting:

$$\mathbf{A} \cdot \mathbf{G}_{\text{corr}} = -\mathbf{A} \cdot \mathbf{G}' - \mathbf{G}_{\text{ext}} . \quad (2.25)$$

If (2.24) is inserted in equation (2.25):

$$\mathbf{A} \cdot \mathbf{Y}' \cdot \mathbf{A}^T \cdot \mathbf{P}_{\text{corr}} = -\mathbf{A} \cdot \mathbf{G}' - \mathbf{G}_{\text{ext}} . \quad (2.26)$$

This expression can be rewritten in a simpler form:

$$\mathbf{H} \cdot \mathbf{P}_{\text{corr}} = \mathbf{d} , \quad (2.27)$$

where

$$\mathbf{H} = \mathbf{A} \cdot \mathbf{Y}' \cdot \mathbf{A}^T \quad \text{and} \quad \mathbf{d} = -\mathbf{A} \cdot \mathbf{G}' - \mathbf{G}_{\text{ext}} .$$

Equation (2.27) can be used to evaluate the pressure correction \mathbf{P}_{corr} , which is then inserted in (2.24) to evaluate also the mass flow rate correction. Then, using (2.21) and (2.22), \mathbf{P} and \mathbf{G} can be evaluated and used as new guesses for the following iterations. These iterations stop when a certain tolerance (which is fixed as input) on the residuals is reached.

Moreover, under-relaxation factors are used to improve the process of convergence. Therefore, equations (2.21) and (2.22) are modified as follow:

$$\mathbf{P} = \mathbf{P}' + \alpha \mathbf{P}_{\text{corr}} , \quad (2.28)$$

$$\mathbf{G} = \mathbf{G}' + \alpha \mathbf{G}_{\text{corr}} . \quad (2.29)$$

Finally, one should take care of the boundary conditions that concern the mass flow rates entering or exiting the network, that are imposed on the vector \mathbf{G}_{ext} , and the pressure which is imposed in at least one node of the vector \mathbf{P}' . Since these values are exact, corrections must not be applied.

To sum up, a schematic of the SIMPLE algorithm, that permits to find the values of mass flow rates in the branches and pressure in the nodes of the district heating network analysed, is depicted in Figure 2.1.

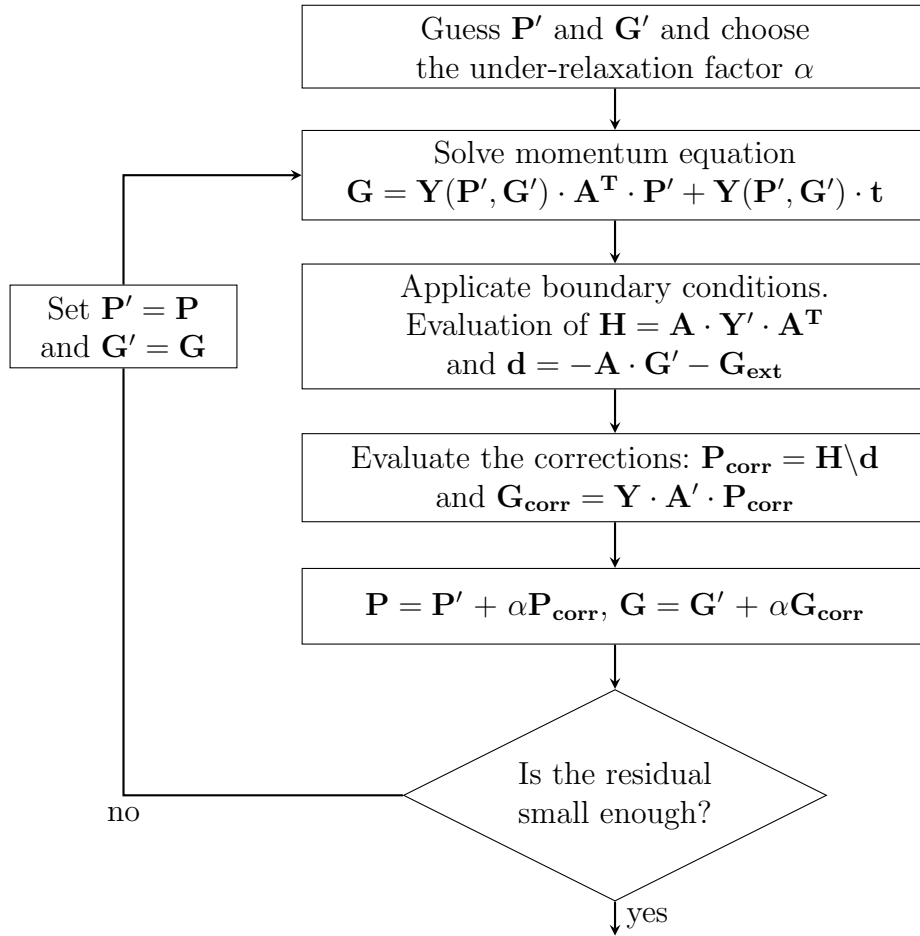


Figure 2.1: Schematic of the SIMPLE algorithm [9].

Chapter 3

The thermal problem

Modelling the thermal behaviour of a District Heating Network means to be able to predict the temperature evolution of each node of the network. Therefore, energy conservation equation must be solved for the whole system. Assuming compressibility effects and viscous heating as negligible, it can be written as:

$$\rho c_p \frac{\partial T}{\partial t} + \rho c_p \mathbf{v} \cdot \nabla T = \nabla \cdot k \nabla T + \varphi_s , \quad (3.1)$$

where the first term is the transient term, the second term represents the advective contribution due to mass flow rates in the branches, the third term is the conductive term and the last one represents the volumetric heat source contribution.

In case of constant properties, equation (3.1) becomes:

$$\frac{(\partial \rho c_p T)}{\partial t} + \nabla \cdot (\rho c_p \mathbf{v} T) = \nabla^2 k T + \varphi_s . \quad (3.2)$$

Moreover, the model can be considered as one-dimensional, so that the energy equation reduces to:

$$\frac{\partial(\rho c_p T)}{\partial t} + \frac{\partial(\rho c_p v_1 T)}{\partial x_1} = k \frac{\partial^2 T}{\partial x_1^2} + \varphi_s . \quad (3.3)$$

In this case, the volumetric heat source φ_s can be split in two terms: φ_v , which takes into account the heat generated within the system, and $-\varphi_l$, taking into account the losses due to the non-adiabatic walls. In fact, the presence of non-adiabatic walls causes temperature gradients in the direction perpendicular to x_1 , and, since in the one-dimensional model these gradients cannot be explicitly considered, they are taken into account by means of a term equivalent to a heat sink. Then, equation (3.3) becomes:

$$\frac{\partial(\rho c_p T)}{\partial t} + \frac{\partial(\rho c_p v_1 T)}{\partial x_1} = k \frac{\partial^2 T}{\partial x_1^2} + \varphi_v - \varphi_l . \quad (3.4)$$

The thermal problem is solved by means of the finite volume method: the energy equation is applied in integral form to all the control volumes of the domain. Each control volume includes the junction node and half of each duct entering or exiting the junction, as depicted in Figure 3.1.

Adiabatic and perfect mixing is assumed when different streams converge in a junction: the temperature of all the flows exiting from the junction are at the same temperature T .

Integrating equation (3.4) over a control volume brings to:

$$\frac{\partial(\rho c_p T_i)}{\partial t} V_i + \sum_{j=1}^{NB} \pm \rho c_p v_1 T_j S_j = \sum_{j=1}^{NB} \pm k \frac{\partial T}{\partial x_1} \Big|_j S_j + \Phi_{v,i} - \Phi_{l,i} , \quad (3.5)$$

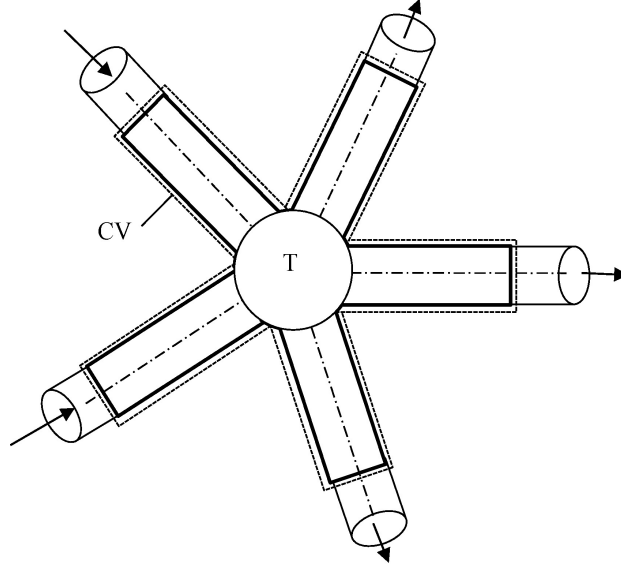


Figure 3.1: Schematic of the control volume of a node [9].

where NB is the total number of branches entering or exiting that control volume, S_j is the cross section of the j -th branch and V_i is the volume of the CV considered, which can be computed as $\sum_{j=1}^{NB} S_j \cdot L_j / 2$. For what concerns the advective and the conductive terms, they are negative if the stream is entering the j -th branch, and positive in the opposite case.

From now on, the conductive term will be neglected, since it is usually small. Also, $\Phi_{v,i}$ is imposed equal to zero. Therefore, the following equation will be considered, remembering that $G = \rho v S$:

$$\frac{\partial(\rho c_p T_i)}{\partial t} V + \sum_{j=1}^{NB} \pm c_p G_j T_j = -\Phi_{l,i} , \quad (3.6)$$

where the term accounting for the heat losses Φ_l can be expressed as

$$\Phi_{l,i} = \sum_{j=1}^{NB} \frac{L_j}{2} \Omega_j U_j (T_i - T_\infty) , \quad (3.7)$$

being Ω_j the perimeter of the j -th branch, U_j the global heat transfer coefficient and T_∞ the external temperature.

Note that the energy equation must be expressed in transient form, since thermal perturbations are slowly transferred: indeed, differently from changes in the flows which are quickly transferred to the network as pressure waves (typically in seconds), they travel at water velocity, which is of the order of few meters per second. Thus, temperature changes generated at the production plant reach end-users, often located after tens of kilometers, with a significant delay, up to several hours. For these reasons, the model adopted is based on a *quasi-dynamic* approach: the flow and the pressure are obtained through a static analysis, while temperature is dynamically evaluated.

From equation (3.6), one can observe that there is a need to define the temperature T_j associated with each boundary of the control volume, i.e. the temperature in the middle point of each branch: it must be expressed as a function of the nodal values of temperature T_i , which are the unknowns of the problem. After that, the equations will be ready to be written in matrix form.

To do this, it would seem natural to apply to the central differencing method, which is known to work well for the diffusion term, even on the convective term. However, while the diffusion process affects the distribution of temperature along its gradients equally in all the directions, excellently fitting this scheme which has such an isotropic nature, the convection process has a very different feature: it is highly anisotropic and affects the solution only in the flow direction. For this reason, the application of the central differencing scheme to the convective term generates some problems, which will be further analysed taking as example of application the convection-diffusion problem.

3.1 The central differencing scheme

3.1.1 Steady-state advection-diffusion model problem

In steady state and if there are no sources, the one-dimensional convection-diffusion problem is governed by the following equation, obtained by a simplification of equation (3.4)¹:

$$\frac{\partial(\rho c_p v T)}{\partial x} = k \frac{\partial^2 T}{\partial x^2} . \quad (3.8)$$

The domain is assumed to be a pipe with constant section in which water flows. Due to the incompressibility constraint, v is constant along the pipe. Integrating equation (3.8) over the control volume represented in Figure 3.2, one can obtain:

$$\rho c_p v S T_e - \rho c_p v S T_w = k S \left. \frac{\partial T}{\partial x} \right|_e - k S \left. \frac{\partial T}{\partial x} \right|_w . \quad (3.9)$$

For a uniform grid, and with a central difference scheme, the cell face values of T can be written as:

$$T_e = \frac{T_P + T_E}{2} \quad T_w = \frac{T_W + T_P}{2} . \quad (3.10)$$

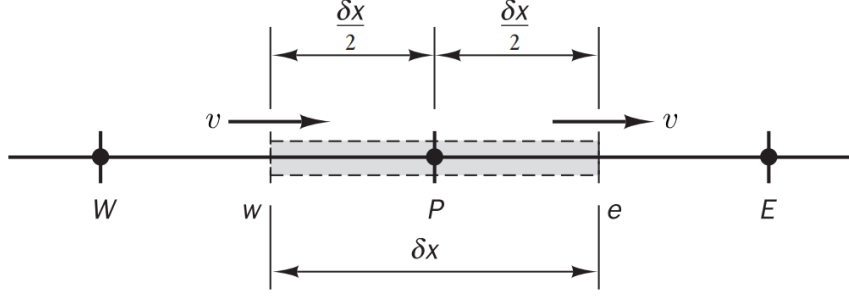
These expressions can be substituted in equation (3.9), that becomes:

$$\rho c_p v \frac{T_P + T_E}{2} - \rho c_p v \frac{T_W + T_P}{2} = k \frac{T_E - T_P}{\delta x} - k \frac{T_P - T_W}{\delta x} . \quad (3.11)$$

Grouping the multipliers, it is possible to end up with the following formulation:

$$-\left(\frac{\rho c_p v}{2} + \frac{k}{\delta x} \right) T_W + \left(\frac{2k}{\delta x} \right) T_P + \left(\frac{\rho c_p v}{2} - \frac{k}{\delta x} \right) T_E = 0 . \quad (3.12)$$

¹For the sake of simplicity from now on it will be considered $x_1 = x$ and $v_1 = v$.


 Figure 3.2: A control volume around node P . Modified from [17].

This discretization equation can be applied to all the internal nodal points, while the control volumes that are adjacent to the domain boundaries need special treatment, since they need to take into account boundary conditions.

Supposing that Dirichlet boundary conditions are applied to the west boundary of the first control volume and to the east boundary of the last control volume, equation (3.9) takes a different form. Indeed, for the first control volume, T_w is known, and the discretization equation reads:

$$\rho c_p v \frac{T_P + T_E}{2} - \rho c_p v T_w = k \frac{T_E - T_P}{\delta x} - k \frac{T_P - T_w}{\delta x/2}. \quad (3.13)$$

Rearranging the various terms, one obtains:

$$\left(\frac{\rho c_p v}{2} + \frac{3k}{\delta x} \right) T_P + \left(\frac{\rho c_p v}{2} - \frac{k}{\delta x} \right) T_E = \left(\rho c_p v + \frac{2k}{\delta x} \right) T_w. \quad (3.14)$$

Similarly, for the last control volume, T_e is known:

$$\rho c_p v T_e - \rho c_p v \frac{T_W + T_P}{2} = k \frac{T_e - T_P}{\delta x/2} - k \frac{T_P - T_W}{\delta x} \quad (3.15)$$

$$\left(-\frac{\rho c_p v}{2} - \frac{k}{\delta x} \right) T_W + \left(-\frac{\rho c_p v}{2} + \frac{3k}{\delta x} \right) T_P = \left(-\rho c_p v + \frac{2k}{\delta x} \right) T_e. \quad (3.16)$$

Then, the whole problem can be written in matrix formulation and the solution \mathbf{T} can be obtained:

$$\mathbf{KT} = \mathbf{f} \quad (3.17)$$

Some example are carried out in order to assess the quality of the results produced by the central differencing scheme. The three cases that are presented differ for number of control volumes N , entity of the advective part $F = \rho c_p v$, entity of the conductive part $D = k/\delta x$, and, clearly, their ratio, which is the Peclet number, defined as:

$$Pe = \frac{\rho c_p v}{\frac{k}{\delta x}} . \quad (3.18)$$

In detail, the data of the three cases are the following ones:

1. $N = 5, F = 0.1 \text{ W}/(m^2K), D = 0.5 \text{ W}/(m^2K) \rightarrow Pe = 0.2$
2. $N = 5, F = 2.5 \text{ W}/(m^2K), D = 0.5 \text{ W}/(m^2K) \rightarrow Pe = 5$
3. $N = 20, F = 2.5 \text{ W}/(m^2K), D = 2 \text{ W}/(m^2K) \rightarrow Pe = 1.25$

The pipe is imposed to be 1 meter long and, as boundary conditions, $T = 100 \text{ }^\circ\text{C}$ is imposed on the left and $T = 0 \text{ }^\circ\text{C}$ on the right.

The results are reported in Figure 3.3, where they are compared to the analytical solution given by:

$$T(x) = c_1 + c_2 \cdot e^{\alpha x}, \quad (3.19)$$

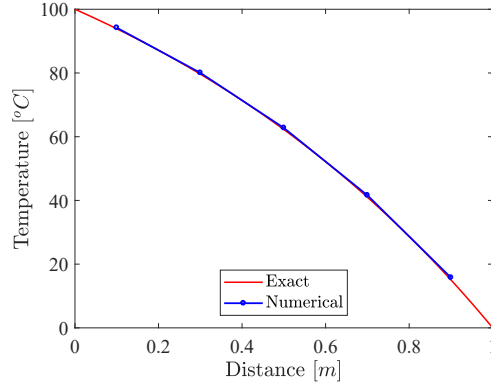
where $c_2 = (T_{left} - T_{right})/(e^{\alpha L} - 1)$, $c_1 = T_{left} - c_2$ and $\alpha = F/(D \cdot \delta x)$. From Figure 3.3(a) it can be seen that in the first case, despite the coarse grid, the numerical solution is able to accurately reproduce the correct one, due to the fact that the advective contribution is sufficiently low with respect to the diffusive one.

With the same grid but with a more significant advective contribution, as in the case of Figure 3.3(b), the numerical solution is completely unphysical: it is no more monotonic, affected by unrealistic oscillations. Taking a finer grid, with the same value of the advective term as in the previous case, the numerical solution is again representative of the physics of the problem, as it is possible to see in Figure 3.3(c). Qualitatively, it is possible to observe that when the problem is strongly affected by advection, a finer grid is needed to be able to produce a relevant numerical solution, due to the fact that the central differencing scheme is isotropic by nature and it is not always able to represent the anisotropy of convection.

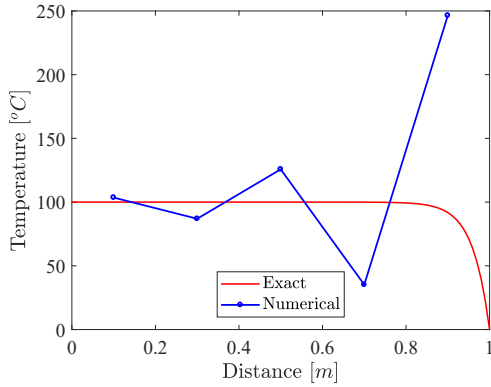
3.1.2 Conservativeness and boundedness

In general, the results produced by a numerical method should reproduce the exact solution when the number of cells is infinitely large, whatever the differencing method used. However, in practical calculations the number of cells should necessarily be limited. For this reason, the choice of the discretization scheme to be adopted assumes a relevant weight: it will be able to produce a result which is physically realistic only if it satisfies certain fundamental properties. The main ones are conservativeness and boundedness. These properties are described in the following lines according to the analysis of [17].

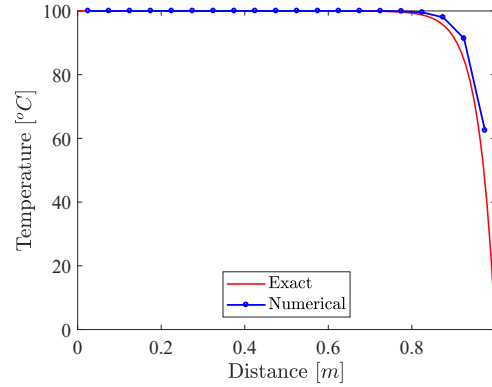
The finite volume formulation is conservative by construction inside the element, but conservation must occur at the element boundary as well. In this sense, a scheme guarantees conservativeness if the energy flux leaving one cell across a certain face is equal to the energy flux entering the adjacent cell through the same face. Conservativeness is always achieved by the central differencing scheme. This can be proved



(a) $Pe = 0.2$



(b) $Pe = 5$



(c) $Pe = 1.25$

Figure 3.3: Numerical CDS solution and exact solution of the one-dimensional steady-state advection-diffusion problem with three different Peclet numbers.

considering the one-dimensional steady-state diffusion problem without sources on the domain represented in Figure 3.4 and writing an overall flux balance which can be obtained by summing the net flux through each control volume:

$$\left[k \frac{T_2 - T_1}{\delta x} - q_A \right] + \left[k \frac{T_3 - T_2}{\delta x} - k \frac{T_2 - T_1}{\delta x} \right] + \left[k \frac{T_4 - T_3}{\delta x} - k \frac{T_3 - T_2}{\delta x} \right] + \left[q_B - k \frac{T_4 - T_3}{\delta x} \right] = q_B - q_A . \quad (3.20)$$

The fluxes are expressed in a consistent manner and cancel out in pairs when summed over the entire domain. Therefore, equation (3.20) expresses the overall conservation of T .

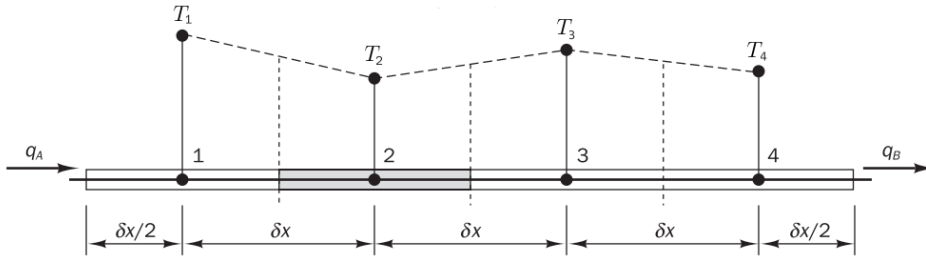


Figure 3.4: Example of consistent specification of diffusive fluxes [17].

For boundedness to be satisfied, two conditions are required:

- In order to guarantee the convergence of the iterative method which solves the set of algebraic equations the Scarborough criterion must be satisfied. It requires that

$$\frac{\sum |a_{nb}|}{|a'_P|} \begin{cases} \leq 1 \text{ for all nodes} \\ < 1 \text{ for at least one node} \end{cases} \quad (3.21)$$

where a'_P is the net coefficient of the central node P , and a_{nb} is the summation over all the neighbouring nodes. Analysing equation (3.12), one can verify that the central differencing scheme satisfies this criterion.

- All the coefficients of the discretized equations written in the form $a_P T_P = a_W T_W + a_E T_E$ should have the same sign. Looking at equation (3.12), it is possible to see that this happens only if:

$$\frac{\rho c_p v}{2} < \frac{k}{\delta x}, \quad (3.22)$$

i.e.:

$$Pe = \frac{\rho c_p v}{\frac{k}{\delta x}} < 2 . \quad (3.23)$$

Therefore, the central differencing scheme is conservative but it is bounded only under the condition that $Pe < 2$, explaining the behaviour of the results seen in Figure 3.3 and confirming that this scheme is not able to reproduce an advective dominant problem with a limited number of nodes. Indeed, in the extreme case of pure advection the Peclet number tends to $+\infty$. Instead, coming back to pure diffusion, $Pe = 0$ and the central differencing scheme accurately describes the real solution.

Due to the instability of the central differencing scheme in advection dominated situations, there is a need to individuate a stable scheme, which is able to describe the strongly anisotropic nature of this phenomenon.

3.2 The upwind scheme

The simplest numerical scheme that solves the problem of stability is the Upwind Differencing Scheme, which takes into account the flow direction of the stream. Using this method, the temperature value at a cell face is taken equal to the one of the upstream node.

3.2.1 Steady-state advection-diffusion model problem

Applying the upwind differencing scheme to the one-dimensional steady-state advection diffusion problem seen in Section 3.1.1 and expressed by equation (3.8)

brings to the following discretized equation, supposing that the flow is in the positive direction:

$$\rho c_p v T_P - \rho c_p v T_W = k \frac{T_E - T_P}{\delta x} - k \frac{T_P - T_W}{\delta x} . \quad (3.24)$$

Grouping the multipliers it is possible to obtain:

$$-\left(\rho c_p v + \frac{k}{\delta x}\right) T_W + \left(\rho c_p v + \frac{2k}{\delta x}\right) T_P - \left(\frac{k}{\delta x}\right) T_E . \quad (3.25)$$

It can be easily shown that the expressions utilised by the upwind differencing scheme to approximate the fluxes across the faces are consistent and therefore that the formulation is conservative.

Moreover, looking at equation (3.25), it is possible to verify that both the Scarborough criterion and the condition on the sign of multipliers are always verified, so boundedness is guaranteed.

Therefore, the upwind differencing scheme gives an answer to the problem of lack of stability of the central differencing scheme in those situations in which advection plays a significant role.

Thanks to its stability and also because of its simplicity, the upwind differencing scheme has been widely applied in CFD calculations in general and in thermo-fluid dynamic models of district heating networks [8] [9].

However, it is important to observe that the introduction of stability comes at the price of a reduced accuracy: while the central differencing scheme was second order accurate, the upwind differencing scheme is only first order. Indeed, writing the

Taylor expansion of the advective term around point P :

$$\rho c_p v T(x) = \rho c_p v T(P) + \left. \frac{\partial(\rho c_p v T)}{\partial x} \right|_P (x - P) + \frac{1}{2} \left. \frac{\partial^2(\rho c_p v T)}{\partial x^2} \right|_P (x - P)^2 + o((x - P)^3) \quad (3.26)$$

and rearranging the terms evaluating the expression in W , one obtains:

$$\left. \frac{\partial(\rho c_p v T)}{\partial x} \right|_P = \frac{\rho c_p v T(P) - \rho c_p v T(W)}{\delta x} - \frac{1}{2} \left. \frac{\partial^2(\rho c_p v T)}{\partial x^2} \right|_P \delta x - o(\delta x^2). \quad (3.27)$$

The first term on the right hand side of equation (3.27) represents exactly the upwind approximation, while the last term is the truncation error. It can be seen that the method is first-order accurate, i.e. the error scales linearly with the grid size. Furthermore, the error scales with the second derivative of the solution, in a similar manner to the diffusion term, introducing in the problem an artificial-numerical diffusivity which is physically not present.

3.2.2 Transient pure advection model problem

An application to the one-dimensional transient pure advection problem is proposed in order to visualize the problem. In absence of sources, the problem reads:

$$\frac{\partial(\rho c_p T)}{\partial t} + \frac{\partial(\rho c_p v T)}{\partial x} = 0. \quad (3.28)$$

The domain is supposed to be a pipe 1 meter long, in which water flows from left to right at $T = 100$ °C and with $v = 1$ m/s, discretized on a uniform grid. At $t < 0$, the temperature of water in the pipe is assumed to be $T = 0$ °C.

The problem is solved with four different grids, each one with a different number of nodes N . A backward Euler scheme is used for time discretization. The results

are shown in Figure 3.5. The effect of the numerical diffusivity introduced by the method is clearly visible in Figure 3.5(a), in which 10 nodes are used, and it tends to be less significant increasing the number of nodes and moving through $N = 1000$ of Figure 3.5(d).

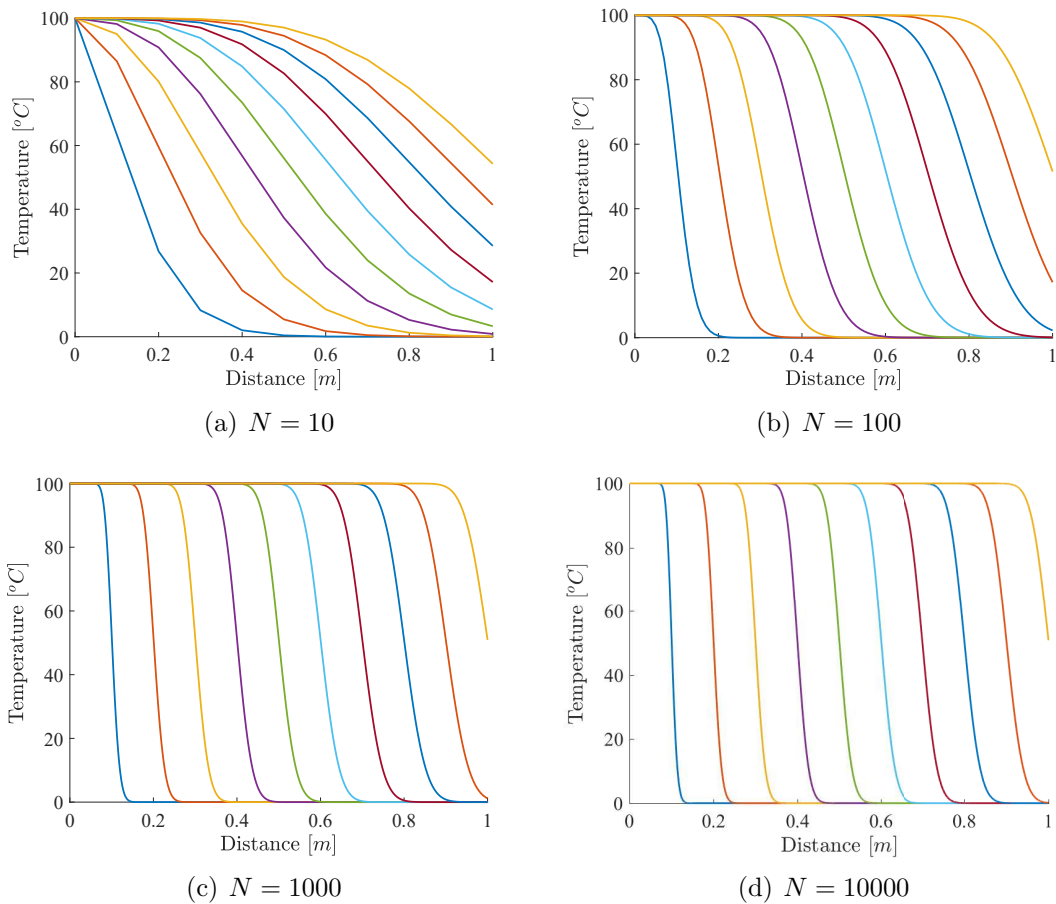


Figure 3.5: Numerical UDS solution of the one-dimensional transient pure advection problem at different times, solved using four grids of different quality.

To better appreciate the differences, in Figure 3.6 the results obtained using the various grid are depicted together with the exact solution at $t = 0.5$ s. It is possible to see that the solution is strongly sensitive to the grid size and in order to obtain

something similar to the analytical solution, at least 1000 nodes are required.

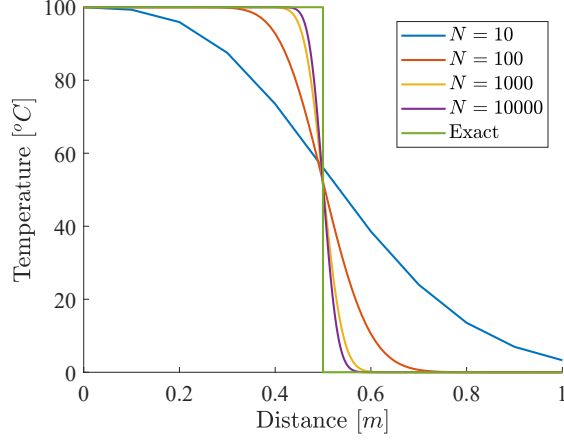


Figure 3.6: Numerical UDS solution of four different grids and exact solution of the one-dimensional transient pure advection problem at $t = 0.5$ s.

The expression of the artificial diffusivity can be easily deduced from equation (3.27):

$$\Gamma_{num} = \frac{v\delta x}{2} . \quad (3.29)$$

Clearly, one way to minimize its contribution is to increase the degree of geometrical discretization, as seen in the previous example. However, if one wishes to make it insignificant in comparison with the physical diffusion coefficient Γ_0 , the condition

$$\frac{\Gamma_{num}}{\Gamma_0} \ll 1$$

is required. This condition brings to:

$$\frac{v\delta x}{2\Gamma_0} \ll 1 \quad \Rightarrow \quad \frac{v\delta x}{2\Gamma_0} \ll 1 \quad \Rightarrow \quad \frac{\rho c_p v \delta x}{2k} \ll 1 ,$$

and consequently to:

$$Pe = \frac{\rho c_p v}{\frac{k}{\delta x}} \ll 2 . \quad (3.30)$$

This condition is much more stringent than the practical stability condition $Pe < 2$ of the central differencing scheme. Since it results to be highly unrealistic in terms of practical calculations, there is a need of finding another way to reduce artificial diffusion, in order to build a method which is more reliable in terms of thermal predictions, essential in problems like the one of district heating networks.

Chapter 4

The problem of numerical diffusion

One of the main issues of numerically solving the thermal differential equation to determine the thermal behaviour of a district heating network is that the numerical scheme typically used, i.e. the upwind differencing scheme, introduces an artificial diffusion which affects the quality of the solution, giving a wrong representation of the problem.

As seen in Chapter 3, one way of minimizing this artificial diffusion is to increase the degree of geometrical discretization. However, this solution is unfeasible in simulations of district heating systems, since the computational cost of simulation becomes in this way highly demanding.

Therefore, other methods to decrease the influence of the numerical diffusion without decreasing too much the grid size are investigated. In particular, a model based on the method of characteristic proposed by [18] is quickly described. Then, the pipe model based on the Type31 model of TRNSYS proposed by [10] and [12] is

briefly illustrated. Finally, the discretization technique based on the quadratic upstream interpolation introduced by [19] is analysed. It will be used in the following chapters for the development of a model for the entire district heating network.

4.1 Method of characteristics

Giraud et al. [18] proposed a Modelica[®] model of the pipe in which the energy balance equation is derived according to the method of characteristics. This method permits to noticeably reduce artificial diffusion speeding up the simulation. In order to understand how it works, it is applied on the pure advection problem with no sources as a simplified example. Assuming constant thermo-physical properties and constant positive velocity v , the problem reads:

$$\frac{\partial T}{\partial t} + v \frac{\partial T}{\partial x} = 0 . \quad (4.1)$$

Equation (4.1) says that the directional derivative $(v,1) \cdot \nabla T = 0$, where $\nabla T = (\frac{\partial T}{\partial x}, \frac{\partial T}{\partial t})$. Consequently, T should be constant on the lines $x - vt = x_0$, where x_0 is the point in which this line intersects the x axis. The speed of this line is v and its slope $1/v$.

Knowing $T(x, t = 0) = f(x)$, one can obtain $T(x, t) = f(x_0) = f(x - vt)$ by rigid translation of the initial function. Therefore, the solution of the problem described by equation (4.1) can be obtained since the initial solution is known. It is represented in Figure 4.1: despite only 100 nodes have been used, the solution appears to be quite accurate.

However, as highlighted by [12], when heat losses are introduced, this approach brings to a still considerable error.

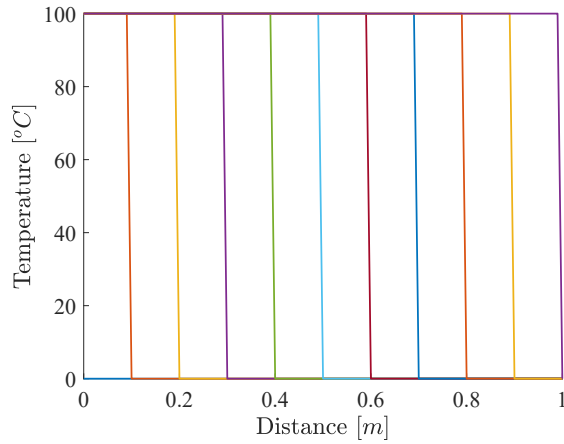


Figure 4.1: Solution of the transient pure advection problem at different times, obtained using the method of characteristics, $N = 100$.

4.2 TRNSYS Type31 Model

Other authors [10] [12] developed a model that relies on the Type31 model of TRNSYS, based on a plug-flow approach. The properties of each fluid particle are considered along their direction in function of time, considering the energy balance in each cell according to Figure 4.2.

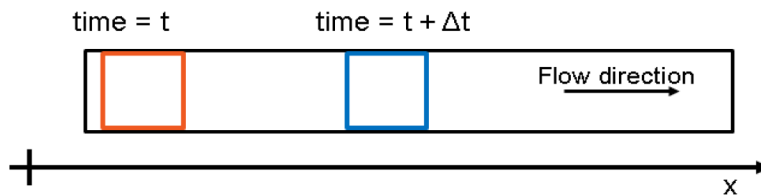


Figure 4.2: Lagrangian coordinate system for one-dimensional system [10].

In this approach, the momentum balance is neglected and the fluid is considered

as incompressible. Therefore, mass and energy balance are expressed by:

$$\frac{\partial m}{\partial t} = 0 , \tag{4.2}$$

$$mc_p \frac{\partial T}{\partial t} = \Phi . \tag{4.3}$$

This component models the thermal behaviour of a flow in a pipe whose cell volume and density are considered as constant. The pipe is divided in cells that follow the heat wave propagation: the entering fluid shifts the position of the existing cell and the energy balance is applied to each cell. The plug-flow model allows a quicker resolution of the system compared to the resolution of 1D finite volume method.

4.3 Quadratic Upstream Interpolation for Convective Kinematics (QUICK)

An alternative strategy to reduce numerical diffusion errors when solving the thermal partial differential equation is to employ higher-order discretization methods which also preserves sensitivity to flow direction to guarantee stability.

The quadratic upstream interpolation for convective kinematics (QUICK) scheme of Leonard [19] uses a three-point upstream-weighted quadratic interpolation for cell values. This formulation leads to the achievement of a conservative formulation with stable advective sensitivity, as proved in the reference.

Considering a uniform grid, the basic interpolation scheme for T_e when v is positive to the right is shown in Figure 4.3 and reads:

$$T_e = \frac{1}{2}(T_P + T_E) - \frac{1}{8}(T_W + T_E - 2T_P) . \tag{4.4}$$

This formulation may be interpreted as a linear interpolation corrected by a term proportional to the upstream-weighted curvature.

For modelling the gradient $(\partial T/\partial x)_e$, the tangent at the wall has also been shown in Figure 4.3. Since for a parabola the slope half way between two points is equal to the slope of the chord joining the points, the gradient is:

$$\left. \frac{\partial T}{\partial x} \right|_e = \frac{T_E - T_P}{\delta x} \quad (4.5)$$

This formula is exactly the same as the central differencing formula. In a similar manner, T_w and $(\partial T/\partial x)_w$, whose construction is represented in Figure 4.4, can be obtained:

$$T_w = \frac{1}{2}(T_W + T_P) - \frac{1}{8}(T_{WW} + T_P - 2T_W) , \quad (4.6)$$

$$\left. \frac{\partial T}{\partial x} \right|_w = \frac{T_P - T_W}{\delta x} . \quad (4.7)$$

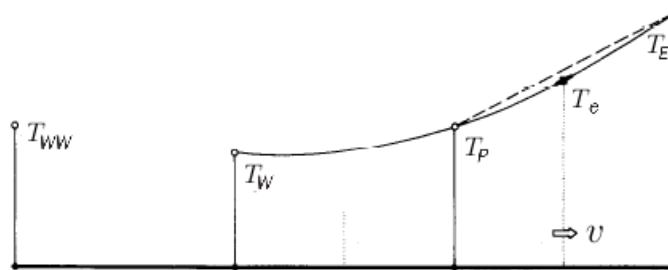


Figure 4.3: Quadratic upstream interpolation for T_e , adapted from [19].

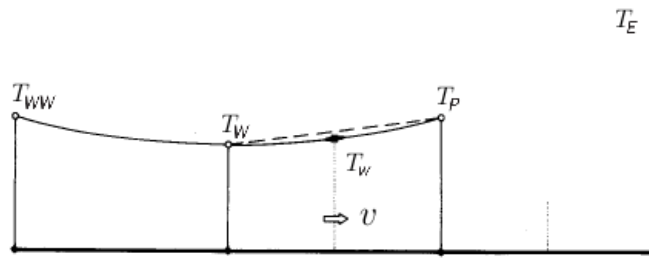


Figure 4.4: Quadratic upstream interpolation for T_w , adapted from [19].

4.3.1 Transient pure-advection model problem

An application of the discretization method previously described on the transient one-dimensional pure-advection problem is proposed in order to see the practical advantages of using this method, comparing the results with the ones obtained with the upwind differencing scheme (see Chapter 3.2.2).

The domain considered is a pipe with constant section, in which water at constant velocity $v = 1 \text{ m/s}$ is flowing from left to right. The initial condition is $T(x,0) = 0$ °C, while the boundary condition, applied to the left boundary, is $T(0,t) = 100$ °C. Backward Euler scheme is used for time discretization. On the last control volume an upwind scheme is used.

In Figure 4.5 the results obtained at different times with different grid sizes are shown. Moreover, Figure 4.6 compares the result obtained at $t = 0.5 \text{ s}$ with the four different meshes. One can see that, using this scheme, a sharper and less sensitive to grid refinement solution is obtained. Indeed, apart from the first case ($N = 10$), the solutions are very close to each other. Small undershoot and overshoot appear, but they are all below 5% of the step length.

In Figure 4.7, the solutions with $N = 100$ and at $t = 0.5 \text{ s}$ of Upwind Differencing Scheme (UDS) and QUICK are compared: in this way it is possible to appreciate how QUICK improves the quality of the solution, leading to a result which is much

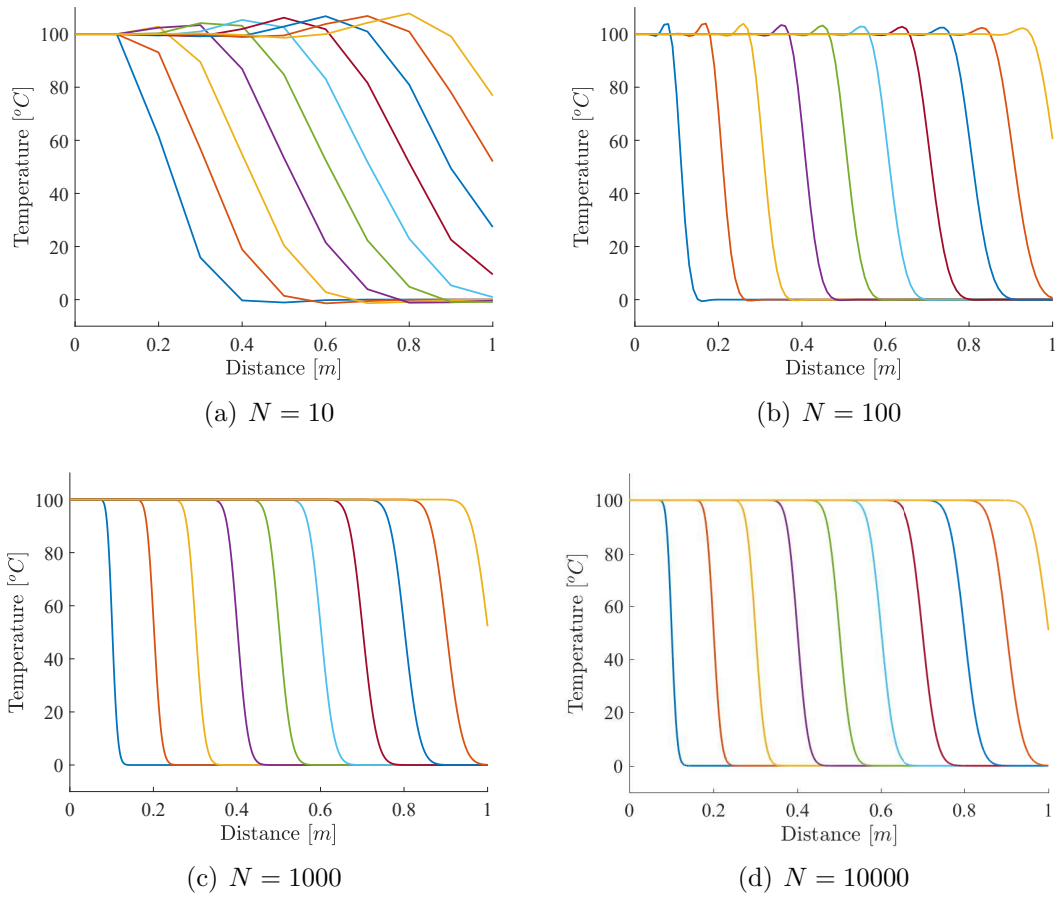


Figure 4.5: Numerical QUICK solution of the one-dimensional transient pure advection problem at different times, solved using four grids of different quality.

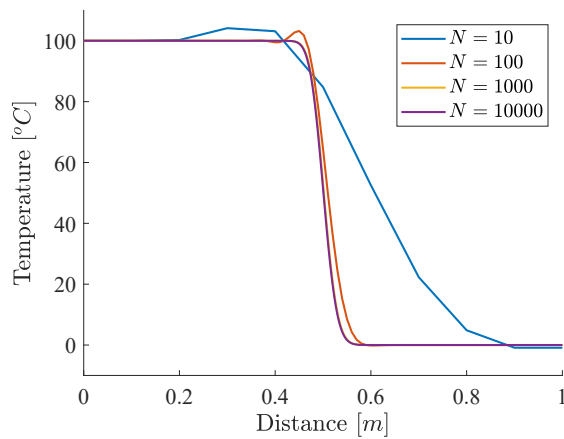


Figure 4.6: Numerical QUICK solution of the one-dimensional transient pure advection problem at $t = 0.5$ s for $N = 10$, $N = 100$, $N = 1000$ and $N = 10000$.

less affected by the artificial diffusion proper to UDS.

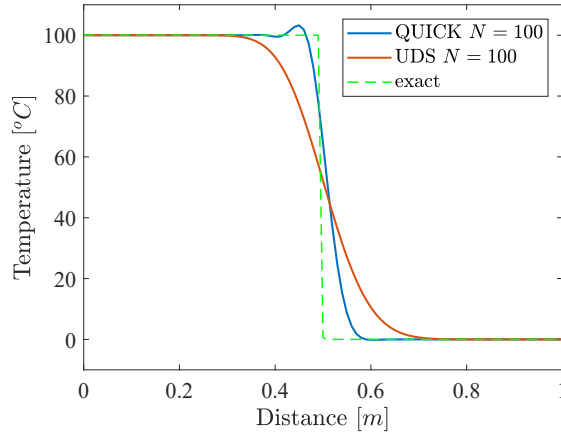


Figure 4.7: Numerical QUICK and UDS solutions compared to the exact one at $t = 0.5$ s and with $N = 100$.

In order to obtain an UDS solution less diffusive and closer to the one produced by QUICK with $N = 100$, at least 1000 nodes are required, as shown in Figure 4.8. Therefore, with respect to the other method, QUICK can produce a solution of comparable accuracy with a great reduction of the number of nodes, and an even more significant reduction of the size of the $N \times N$ matrices.

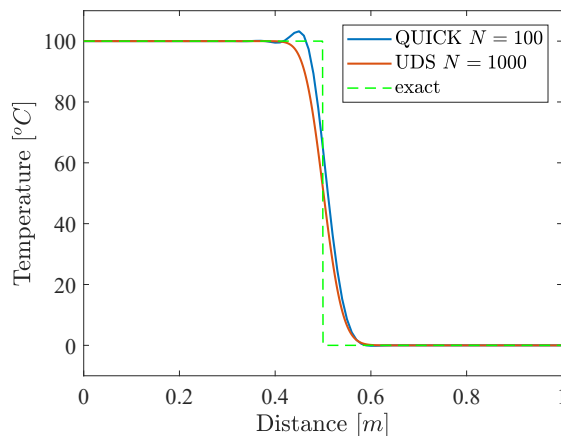


Figure 4.8: Numerical QUICK ($N = 100$) and UDS ($N = 1000$) solutions compared to the exact one at $t = 0.5$ s.

For these reasons, QUICK can be a good solution to decrease the numerical diffusion without increasing too much the computational cost. It can be used as discretization scheme in district heating applications, in order to make the model more reliable than the classically used models in which UDS is implemented, keeping the total cost of computation below the one normally required. The idea of extending the use of this scheme to the whole network will be exploited in the following chapters.

Chapter 5

Adaptive moving mesh methods

The solution of the energy conservation equation for an advection dominated flow in a pipe, and in general in the framework of DHN, has large variations occurring over a small portion of the physical domain. This feature of the solution brings to the need of having a fine mesh in those portions of the domain. If a uniform mesh is used, the number of mesh points becomes very large and the computational cost extremely high.

To cope with this problem, an idea could be to use a non-uniform mesh, placing a high proportion of mesh points in the regions of large solution variation and few points in the rest of the domain, where the solution is less subject to variations. With this basic idea of “mesh adaptivity”, much less mesh points are required with respect to a uniform mesh, and the computational time is significantly reduced.

However, in applications like the one of district heating network, whose thermal behaviour is described by a time-dependent PDE, it is required that the mesh points are dynamically adjusted to follow the front as it propagates in time. This is the concept of “adaptive moving mesh”.

In this chapter an introduction to the principles of adaptive mesh movement in $1D$

is presented, on the basis of what analysed by Huang and Russell in [20].

When approximating the function T by using its values at a finite number of mesh points, a *mesh density function* $\rho(x)$ is chosen in order to distribute these points: mesh points are then collocated in such a way that distance between them are smaller in regions where $\rho(x)$ is larger, and the distances are larger in regions where $\rho(x)$ is smaller. Mesh density functions are also called by other references (e.g. [21]) *monitor functions*. They need to be selected accurately according to the application.

Given an integer $N > 1$ and a continuous function $\rho = \rho(x) > 0$ on a bounded interval $[a, b]$, a mesh $\mathcal{T}_h : x_1 = a < x_2 < \dots < x_N = b$ which evenly distributes ρ among the subintervals determined by the mesh points, in the sense that:

$$\int_{x_1}^{x_2} \rho(x) dx = \dots = \int_{x_{N-1}}^{x_N} \rho(x) dx , \quad (5.1)$$

is an *equidistributing mesh*. In the one-dimensional case, equidistribution plays an important role in mesh adaption. As proved in [20], for a given integer $N > 0$ there exists a unique equidistributing mesh of N point satisfying (5.1) for any strictly positive mesh density function.

For the numerical solution of time-dependent problems, the mesh density function will depend upon the solution, and hence on time. Therefore, it is needed to adopt a time-dependent mesh as well. This moving mesh can be obtained by solving a moving mesh PDE (MMPDE), which is a mesh equation involving mesh speed and defining the co-ordinate transformation.

There are numerous ways of formulating MMPDEs. Some of the most popular formulations are MMPDE4, MMPDE5 and MMPDE6.

Once the new grid has been obtained, it is needed to update the solution T at the

new grid point, based on the knowledge of the solution computed at the old grid point and of the coordinates of the new grid points and of the old ones, as well explained in [22].

This is done by means of a linear interpolation, whose major difficulty generally consists in point location, i.e. finding the elements that contain the new mesh points. For the general situation in which the meshes may have different topologies, this can be quite difficult, representing a topic of active research on its own right. However, the case treated here is much simpler: the new and old meshes have the same topology, so that the new mesh can be interpreted as a deformation of the old one. The search for the location of a mesh point begins with the neighbours of the corresponding point on the old mesh, and it proceeds until the element that contains the new point is found. Typically it is not so far from the old point and the point location is quickly identified.

5.1 Transient pure advection model problem

In order to appreciate the advantages of using such a kind of method, an application to the transient pure advection model problem, described by equation (3.28) and previously analysed with UDS and QUICK on a uniform grid, is proposed.

Data are the same of the previous cases, and the only thing that changes is that now the grid is non-uniform and it evolves with time, as the front propagates.

The mesh density function used to distribute the mesh points is the arc-length mesh density function:

$$\rho = \sqrt{1 + |\nabla T|^2} . \tag{5.2}$$

This mesh density function is one of the most used in moving mesh applications. It aims at equidistributing the arc-length of the solution curve over the mesh points. The algorithm chosen to generate the new mesh at each new instant of time is the MMPDE5 [23]. After having built the new mesh, which is updated at each time, one needs to discretize the equation in space and then in time, in order to be able to write the discretized problem in matrix form and to solve it.

The mesh in this case is no more uniform, and it is evolving in time. Equation (3.28) integrated on a generic control volume reads:

$$\frac{\partial(\rho c_p T)}{\partial t} V + \rho c_p v S T_e - \rho c_p v S T_w = 0. \quad (5.3)$$

By simplification, one obtains:

$$\frac{\partial(\rho c_p T)}{\partial t} (x_e - x_w) + \rho c_p v T_e - \rho c_p v S T_w = 0. \quad (5.4)$$

In fact, there is no more a constant δx valid for all the cells, but it varies for each node and also at each time. Since the faces are assumed to be in the mid point between the two nodes, their coordinates are:

$$x_e = \frac{x_P + x_E}{2} \quad \text{and} \quad x_w = \frac{x_W + x_P}{2}. \quad (5.5)$$

Therefore:

$$x_e - x_w = \frac{x_P + x_E}{2} - \frac{x_W + x_P}{2} = \frac{x_E - x_W}{2}. \quad (5.6)$$

For what concerns the values of the solution at the cell faces, their evaluation depends on the discretization scheme chosen.

5.1.1 Upwind differencing scheme

If the upwind differencing scheme is used, the values of T at the cell faces are imposed equal to their upstream value, as in the uniform mesh case. In this problem, since the flow is considered positive to the right, $T_e = T_P$ and $T_w = T_W$.

The solution produced by UDS with an adaptive moving mesh made of 100 nodes is shown in Figure 5.1(a), where the temperature behaviour every 0.1 s is reported; to have an idea of the movement of the mesh, the centroids of the corresponding control volumes are depicted in Figure 5.1(b).

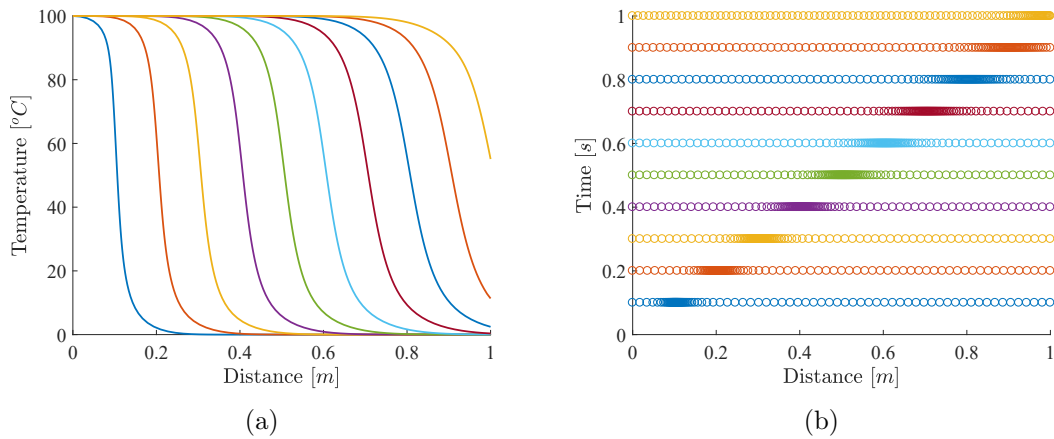


Figure 5.1: On the left, numerical UDS solution on a non-uniform adaptive grid of the one-dimensional transient pure advection problem every 0.1 s. On the right, the centroids of the corresponding adaptive moving mesh.

To understand the benefits of the use of adaptive moving mesh methods, Figure 5.2 compares the numerical solution obtained on the adaptive grid with the one obtained with the uniform grid at $t = 0.5$ s. As expected from expression (3.29), since the numerical diffusivity depends on δx , a more accurate and less over-diffusive solution is obtained with the adaptive grid in the gradient zone, where δx diminishes with respect to the uniform grid. There are other portions of the domain where δx increases and consequently an additional numerical diffusivity is added; however,

in these zones the solution is flatter and the introduction of a numerical diffusivity is less critical. Overall, the use of an adaptive grid can be considered satisfactory.

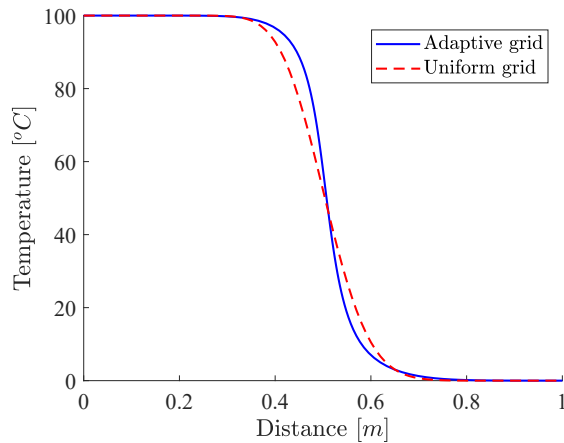


Figure 5.2: Numerical UDS solution of the one-dimensional transient pure advection problem on an adaptive grid and on a uniform one, at $t = 0.5$ s.

5.1.2 QUICK

The solution values at the cell faces can also be obtained through a three-point upstream-weighted quadratic interpolation (QUICK). However, in the case of the intrinsically non-uniform adaptive mesh, the formulations of the wall values expressed by equations (4.4) and (4.6) are no more valid. Indeed, those simplified expressions were obtained due to the fact that the mesh was uniform and δx constant all over the domain. As an example, to obtain the upstream quadratic interpolation on a non-uniform grid of the wall value T_e of a certain control volume, one might first of all find the equation of the parabola passing through the three points W , P and E (since the flow is positive to the left), by solving for a_e , b_e and c_e the

following system:

$$\begin{cases} T_W = a_e x_W^2 + b_e x_W + c_e \\ T_P = a_e x_P^2 + b_e x_P + c_e \\ T_E = a_e x_E^2 + b_e x_E + c_e . \end{cases} \quad (5.7)$$

In this way, each coefficient can be evaluated as a function of the nodal values of the solution and of the coordinate of the centroids:

$$a_e = \begin{bmatrix} -\frac{1}{(x_W - x_E)(x_P - x_W)} \end{bmatrix} T_W + \begin{bmatrix} \frac{1}{(x_W - x_E)(x_P - x_W)} + \frac{1}{(x_W - x_E)(x_E - x_P)} \end{bmatrix} T_P + \begin{bmatrix} -\frac{1}{(x_W - x_E)(x_E - x_P)} \end{bmatrix} T_E$$

$$b_e = \begin{bmatrix} -\frac{1}{x_P - x_W} + \frac{x_P + x_W}{(x_W - x_E)(x_P - x_W)} \end{bmatrix} T_W + \begin{bmatrix} \frac{1}{(x_P - x_W)} - \frac{x_P + x_W}{(x_W - x_E)(x_P - x_W)} - \frac{x_P + x_W}{(x_W - x_E)(x_E - x_P)} \end{bmatrix} T_P + \begin{bmatrix} \frac{x_P + x_W}{(x_W - x_E)(x_E - x_P)} \end{bmatrix} T_E$$

$$c_e = \begin{bmatrix} 1 + \frac{x_W^2}{(x_W - x_E)(x_P - x_W)} + \frac{x_W}{x_P - x_W} - \frac{(x_P + x_W)x_W}{(x_W - x_E)(x_P - x_W)} \end{bmatrix} T_W + \begin{bmatrix} -\frac{x_W^2}{(x_W - x_E)(x_P - x_W)} - \frac{x_W^2}{(x_W - x_E)(x_E - x_P)} - \frac{x_W}{x_P - x_W} + \frac{(x_P + x_W)x_W}{(x_W - x_E)(x_P - x_W)} + \frac{(x_P + x_W)x_W}{(x_W - x_E)(x_E - x_P)} \end{bmatrix} T_P + \begin{bmatrix} \frac{x_W^2}{(x_W - x_E)(x_E - x_P)} - \frac{(x_P + x_W)x_W}{(x_W - x_P)(x_E - x_P)} \end{bmatrix} T_E$$

At this point, T_e can be obtained by simply evaluating:

$$T_e = a_e x_e^2 + b_e x_e + c_e , \quad (5.8)$$

being x_e expressed by (5.5). Similarly, T_w can be expressed knowing the values of the solution in the points WW , W and P and by finding the equation of another parabola whose coefficients are a_w , b_w and c_w :

$$\begin{cases} T_{WW} = a_w x_{WW}^2 + b_w x_{WW} + c_w \\ T_W = a_w x_W^2 + b_w x_W + c_w \\ T_P = a_w x_P^2 + b_w x_P + c_w , \end{cases} \quad (5.9)$$

$$T_w = a_w x_w^2 + b_w x_w + c_w . \quad (5.10)$$

Obviously, for the non-uniform adaptive grid these coefficients are not always the same but they vary for each control volume and at each time step.

After these steps, the problem can be written in matrix form and it is ready to be solved. Figure 5.3(a) illustrates the solution every 0.1 s for a non-uniform adaptive grid made of 100 nodes. In Figure 5.3(b) the corresponding evolving grid is plotted. It is possible to appreciate a noticeable reduction of the undershoot and overshoot that were present in uniform mesh case: now they are all below 1%. Solutions obtained with the uniform mesh and with the adaptive moving mesh are compared in Figure 5.4.

In conclusion, the introduction of an adaptive moving mesh method seems to bring

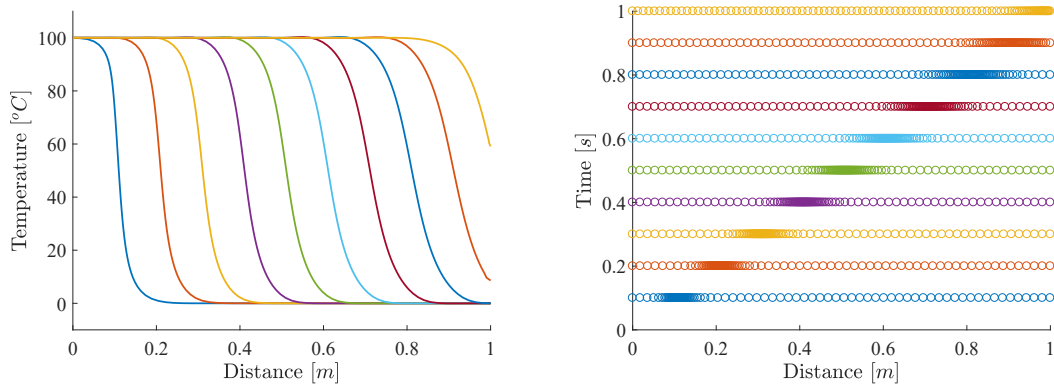


Figure 5.3: On the left, numerical QUICK solution on a non-uniform adaptive grid of the one-dimensional transient pure advection problem every 0.1 s. On the right, the centroids of the corresponding adaptive moving mesh.

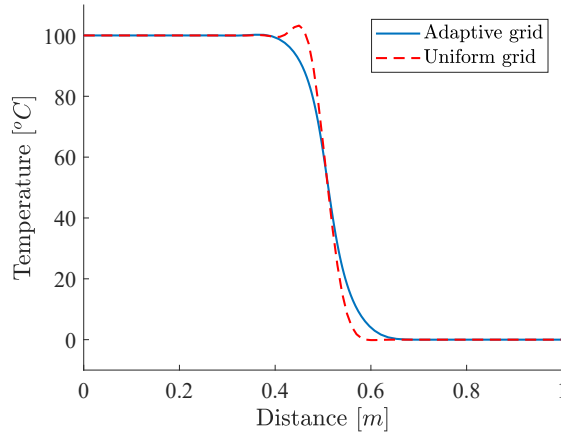


Figure 5.4: Numerical QUICK solution of the one-dimensional transient pure advection problem on an adaptive grid and on a uniform one, at $t = 0.5$ s.

to favourable results. It leads to the correction of the main issues related to the scheme used to approximate the wall values, being in the UDS case the numerical diffusivity and in QUICK the presence of overshoots. Therefore, one can think to extend the use of adaptive moving mesh methods to the whole district heating network, in order to guarantee a more accurate prediction of what happens in reality. To avoid to make the analysis too heavy, the model proposed in this work and analysed in the following chapters is not based on a method of this kind. However,

for the mentioned benefits, the application of moving grids within district heating networks can be left as a target for future works.

Chapter 6

Description of the thermal model

In view of what seen in the previous chapters, the thermal model proposed is mainly based on the QUICK scheme, in order to reduce the undesired effect of the artificial diffusion. Starting from the initial topology description of the district heating network, the configuration is modified by adding some “fictitious” nodes to the “real” ones.

This choice aims at decreasing the size of the control volumes to increase the accuracy of the solution thanks to the improvement of spacial discretization. Moreover, it helps to have the same mesh size along a physical branch, making the application of QUICK immediate.

The Upwind Differencing Scheme is instead applied to those nodes that were presents in the initial configuration, representing the junctions, and in the previous and the following ones. Indeed, in these nodes, the application of QUICK can generate problems: for instance, the approximation of the control volume face values requires two upstream and one downstream nodes, and the farthest upstream node in case of converging branches is not well defined.

Therefore, the discretization method adopted is actually an hybrid between QUICK

and UDS, but, if a sufficient number of fictitious nodes is added, the percentage of control volumes for which QUICK is adopted is far greater.

As well explained in Chapter 3, the energy conservation equation that models the district heating network, integrated on a generic control volume, reads:

$$\frac{\partial(\rho c_p T_i)}{\partial t} V_i + \sum_{j=1}^{NB} \pm c_p G_j T_j = - \sum_{j=1}^{NB} \frac{L_j}{2} \Omega_j U_j (T_i - T_\infty), \quad (6.1)$$

where NB is the total number of branches entering or exiting that control volume and V_i is the volume of the CV considered, which can be computed as $\sum_{j=1}^{NB} S_j \cdot L_j / 2$, being S_j the cross section of the j -th branch and L_j its length. Ω_j is the perimeter of the j -th branch, U_j the global heat transfer coefficient and T_∞ the external temperature. For what concerns the advective term, it is negative if the stream is entering the j -th branch, and positive in the opposite case.

Equation (6.1) can be discretized using the backward Euler method:

$$\frac{\rho c_p T_i^t - \rho c_p T_i^{t-\Delta t}}{\Delta t} V_i + \sum_{j=1}^{NB} \pm c_p G_j T_j^t = - \sum_{j=1}^{NB} \frac{L_j}{2} \Omega_j U_j (T_i^t - T_\infty), \quad (6.2)$$

The crucial point of the thermal analysis consists now in the approximation of the wall values T_j in terms of nodal values T_i . Once this approximation is done for all the control volumes of the domain, one is able to write a system of equations in matrix form:

$$(\mathbf{M} + \mathbf{K}) \cdot \mathbf{T}^t = \mathbf{f} + \mathbf{M} \cdot \mathbf{T}^{t-\Delta t}, \quad (6.3)$$

and to solve the thermal problem at each instant of time. In expression (6.3), \mathbf{K} is the stiffness matrix and depends on the scheme used to approximate T_j and on the topology of the network. Its construction will be explained in the following sections.

\mathbf{M} is instead a diagonal matrix of dimensions $(N \times N)$, where N is the total number of nodes, whose terms are

$$M_{i,i} = \frac{\rho c_p V_i}{\Delta t}.$$

Finally, \mathbf{f} is a column vector $(N \times 1)$ and represents the known term accounting for the losses:

$$f_i = \sum_{j=1}^{NB} \frac{L_j}{2} \Omega_j U_j T_\infty$$

.

The mass flow rates G_j flowing in the different branches of the network are assumed to be known and fixed (they can be obtained through the SIMPLE algorithm that solves the fluid-dynamic problem and that was illustrated in section 2.3). Therefore, starting from an initial condition, and after having applied proper boundary conditions on the matrix problem, it can be solved step by step as:

$$\mathbf{T}^t = (\mathbf{M} + \mathbf{K}) \setminus (\mathbf{f} + \mathbf{M} \cdot \mathbf{T}^{t-\Delta t}). \quad (6.4)$$

6.1 Approximation of wall values with QUICK

Considering a generic internal control volume, i.e. one of those corresponding to the “fictitious” nodes added to produce a better solution, the approximation of the solution values at the wall of these elements is made by applying the Quadratic Interpolation Scheme for Convective Kinematics proposed by Leonard [19] and explained in section 4.3.

These fictitious nodes in which QUICK is applied do not represent a junction. They are all internal nodes belonging to a pipe. This means that they all have only one incoming and one outgoing fictitious branch.

Calling i the node which represents the center of the generic control volume, and $i - 2$, $i - 1$ and $i + 1$ respectively the two upstream nodes and the downstream one, and considering that the incoming branch is j and the outgoing one $j + 1$, equation (6.2) can be written as:

$$\begin{aligned} \frac{\rho c_p T_i^t - \rho c_p T_i^{t-\Delta t}}{\Delta t} V_i - c_p G_j \left(-\frac{1}{8} T_{i-2}^t + \frac{3}{4} T_{i-1}^t + \frac{3}{8} T_i^t \right) + c_p G_{j+1} \left(-\frac{1}{8} T_{i-i}^t + \frac{3}{4} T_i^t + \frac{3}{8} T_{i+1}^t \right) \\ = -\frac{L_j}{2} \Omega_j U_j (T_i^t - T_\infty) - \frac{L_{j+1}}{2} \Omega_{j+1} U_{j+1} (T_i^t - T_\infty) . \end{aligned} \quad (6.5)$$

This helps to understand how to build the stiffness matrix \mathbf{K} . Indeed, from equation (6.5) it is possible to deduce that at each i -th row corresponding to the i -th control volume, the stiffness matrix has non-zero values in the following positions:

- in the column corresponding to the node before the one that precedes the CV considered, that in the example considered is $i - 2$, where it assumes the value

$$K_{i,i-2} = \frac{1}{8} c_p G_j ;$$

- in the column corresponding to the node that precedes the CV considered, that in the example considered is $i - 1$, where it is

$$K_{i,i-1} = -\frac{3}{4} c_p G_j - \frac{1}{8} c_p G_{j+1} ;$$

- in the column corresponding to the i -th CV considered

$$K_{i,i} = -\frac{3}{8} c_p G_j + \frac{3}{4} c_p G_{j+1} + \frac{L_j}{2} \Omega_j U_j + \frac{L_{j+1}}{2} \Omega_{j+1} U_{j+1} ;$$

- in the column corresponding to the node that follows the CV considered, that in the case analysed is $i + 1$

$$K_{i,i+1} = \frac{3}{8}c_p G_{j+1} .$$

Therefore, for each row the matrix has four non-zero values. Their collocation depends on the enumeration of the nodes. Obviously, they cannot be all subsequent due to the fact that more than one branch can come out from a node and more than one branch can converge in a single node. Anyway, when possible, they are enumerated consecutively to try to obtain a structure as much diagonally dominant as possible.

6.2 Approximation of wall values with USD

For what concerns the nodes corresponding to junctions, the previous and the successive ones, their wall values are not approximated using QUICK. Indeed, this scheme seems to create troubles in the approximation of the solution on the east face of the junction control volume and on the west face of the successive one, which are coincident, especially in the case in which more than one branch converges in a single node. These troubles originate from the fact that in the mentioned face the value of the solution in the farthest of the two upstream nodes, which is needed in QUICK, is not unique when more branches converge in the control volume. For these reasons, to avoid any kind of issues, in these nodes the Upwind Differencing Scheme is used.

To have an idea of how to fill the matrix \mathbf{K} in the row corresponding to these special nodes, an example is proposed. The example is referred to Figure 6.1: there

are two incoming and two outgoing branches for a single control volume centered in node i .

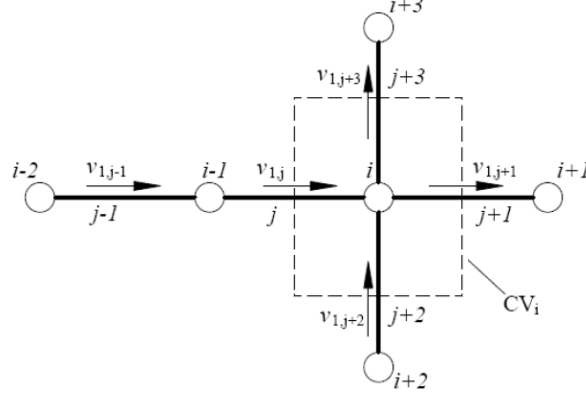


Figure 6.1: Example of the upwind scheme for a node [11].

Therefore, equation (6.2) reads:

$$\begin{aligned} \frac{\rho c_p T_i^t - \rho c_p T_i^{t-\Delta t}}{\Delta t} V_i - c_p G_j T_j^t - c_p G_{j+2} T_{j+2}^t + c_p G_{j+1} T_{j+1}^t + c_p G_{j+3} T_{j+3}^t = \\ -\frac{L_j}{2} \Omega_j U_j (T_i^t - T_\infty) - \frac{L_{j+2}}{2} \Omega_{j+2} U_{j+2} (T_i^t - T_\infty) \quad (6.6) \\ -\frac{L_{j+1}}{2} \Omega_{j+1} U_{j+1} (T_i^t - T_\infty) - \frac{L_{j+3}}{2} \Omega_{j+3} U_{j+3} (T_i^t - T_\infty), \end{aligned}$$

and applying the upwind scheme:

$$\begin{aligned} \frac{\rho c_p T_i^t - \rho c_p T_i^{t-\Delta t}}{\Delta t} V_i - c_p G_j T_{i-1}^t - c_p G_{j+2} T_{i+2}^t + c_p G_{j+1} T_i^t + c_p G_{j+3} T_i^t = \\ -\frac{L_j}{2} \Omega_j U_j (T_i^t - T_\infty) - \frac{L_{j+2}}{2} \Omega_{j+2} U_{j+2} (T_i^t - T_\infty) \quad (6.7) \\ -\frac{L_{j+1}}{2} \Omega_{j+1} U_{j+1} (T_i^t - T_\infty) - \frac{L_{j+3}}{2} \Omega_{j+3} U_{j+3} (T_i^t - T_\infty), \end{aligned}$$

Then, the rows of the matrix \mathbf{K} corresponding to the control volumes that need to be discretized with UDS have non-zero terms in the following positions:

- in the columns corresponding to the control volumes that precede the control

volume i considered, that in this example corresponds to $i - 1$ and $i + 2$

$$K_{i,i-1} = -c_p G_j ,$$

$$K_{i,i+2} = -c_p G_{j+2} ;$$

- in the column corresponding to the control volume i considered, in which the outgoing mass flow rates and all the losses are taken into account; in this case

$$K_{i,i} = c_p G_{j+1} + c_p G_{j+3} + \frac{L_j}{2} \Omega_j U_j + \frac{L_{j+2}}{2} \Omega_{j+2} U_{j+2} + \frac{L_{j+1}}{2} \Omega_{j+1} U_{j+1} + \frac{L_{j+3}}{2} \Omega_{j+3} U_{j+3} .$$

Finally, special care must be taken also to the outlet nodes. In these nodes not only UDS scheme is used, but differently from the previous ones it is needed to pay attention to keep into account the energy extraction.

6.3 Example of application

An example of application is provided in order to test the method proposed. The node-branch representation of the supply line of the district heating network is shown in Figure 6.2. The figure and the data of the district heating network used in this section are taken from [11]. Node 0 represents the power plant that supplies heat to the system, while nodes 7, 12, 13, 14, 16, 18 and 19 are the users, each one requiring a certain amount of thermal demand, and therefore a certain amount of mass flow rate of hot water.

In this example the design of the network is supposed to be known. In particular, the length of the branches, their diameters and their local loss coefficients are detailed in Table 6.1. The friction factor is assumed to be $f = 0.014$. The mass flow

rates required by the users are listed in Table 6.2. At the thermal plant a pressure of 8 *bar* and a temperature of 120 °C are imposed. As initial condition $T = 70$ °C is considered.

In accordance to the method described, some fictitious nodes are added. In detail, a node every 10 *m* is inserted.

The simulation is carried for a total time of 1 hour, and a time step of 1 *s* is used.

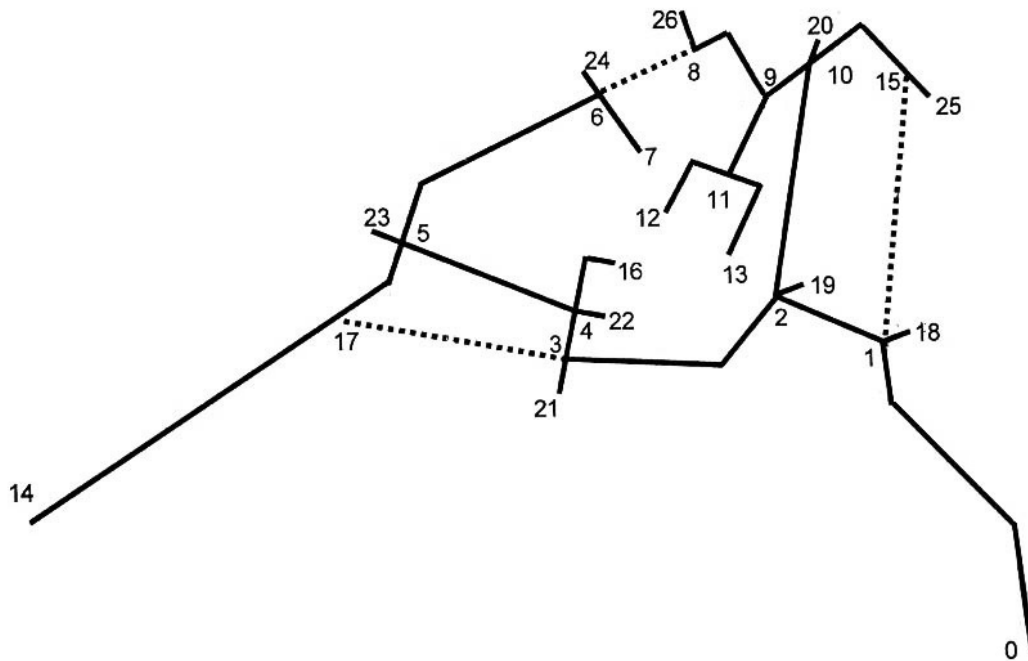


Figure 6.2: Schematic of the district heating network [11].

The model proposed permits to evaluate the temperature evolution of all the nodes. In this way it is possible to obtain the temperature level at the point and at the time desired.

The temperature distribution in those nodes that were presents in the initial topological description of the network is reported in Figures 6.3 and 6.4, respectively after half an hour and after an hour. Note that the colour bars are different. From the comparison of the two pictures one can note that while after half an hour the

Table 6.1: Length, diameter and total local loss coefficient of the various branch of the network [11].

Branch	$L [m]$	$D [mm]$	$\sum_k \beta_k$	Branch	$L [m]$	$D [mm]$	$\sum_k \beta_k$
0 1	660	500	2.6	4 16	240	300	2.9
1 2	260	500	4	10 15	330	125	4.9
2 10	360	350	4	1 15	380	250	4
2 3	500	450	4.3	3 17	400	250	4
3 4	100	450	4	17 14	720	250	2
4 5	380	350	4	1 18	20	125	2
5 6	400	250	4.3	2 19	20	250	2
6 7	140	250	2	10 20	20	250	2
6 8	300	250	4	3 21	20	75	2
9 8	180	250	3.8	4 22	20	250	2
10 9	60	350	4	5 23	50	250	2
9 11	180	250	4	6 24	50	250	2
11 12	160	250	2.9	15 25	50	125	2
11 13	120	250	2.9	8 26	70	250	2
5 17	180	250	4.3				

Table 6.2: Mass flow rates injected in the plant and required by the users [11].

Node	$G [kg/s]$	Node	$G [kg/s]$
0	-513.13	20	36.22
7	23.71	21	3.88
12	27.6	22	58.21
13	32.34	23	70.72
14	31.05	24	30.61
16	78.92	25	18.97
18	15.52	26	28.46
19	56.92		

high temperature mass flow rate started from the power plant at $t = 0 s$ has not yet reached the farthest nodes, after an hour it reaches all the users with a slightly lower temperature due to the heat losses.

Figure 6.5 the temperature evolution of node 14, that represents the farthest user, is illustrated: the hot fluid arrives at this user with about 40 *min* of delay with respect to the power plant.

Then, the same simulation is repeated decreasing the grid size, by imposing a fictitious node every 5 m instead of 10 m . Temperature distributions at $t = 1800 s$ and $t = 3600 s$ are shown in Figures 6.6 and 6.7. The temperature evolution of node 14 is depicted in Figure 6.8. The pictures are similar, but it is possible to immediately see that the overshoot typical of QUICK that was visible in Figure 6.5 is disappeared, improving the quality of the solution. This is obtained at the expenses of the computational time of simulation, which is almost doubled.

In conclusion, the method proposed seems to work well in case of district heating networks, giving a good opportunity to produce a more accurate solution without increasing too much the computational cost.

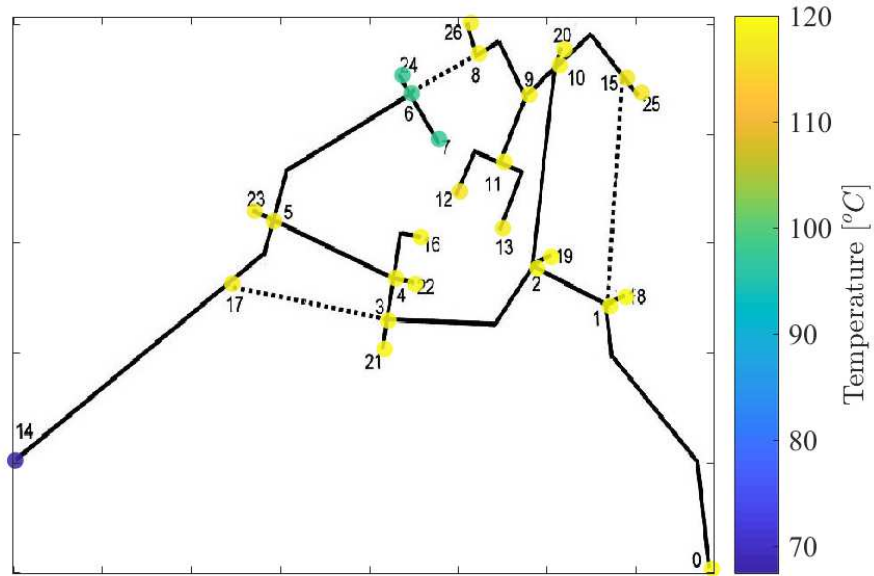


Figure 6.3: Temperature distribution at $t = 1800\text{ s}$ in the *real* nodes, obtained inserting a *fictitious* node every 10 m and using a time step of 1 s .

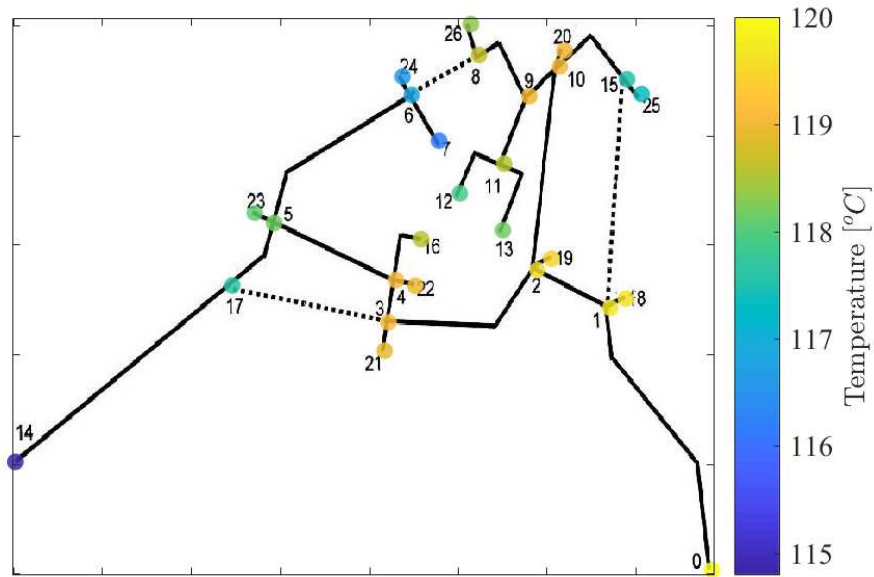


Figure 6.4: Temperature distribution at $t = 3600\text{ s}$ in the *real* nodes, obtained inserting a *fictitious* node every 10 m and using a time step of 1 s .

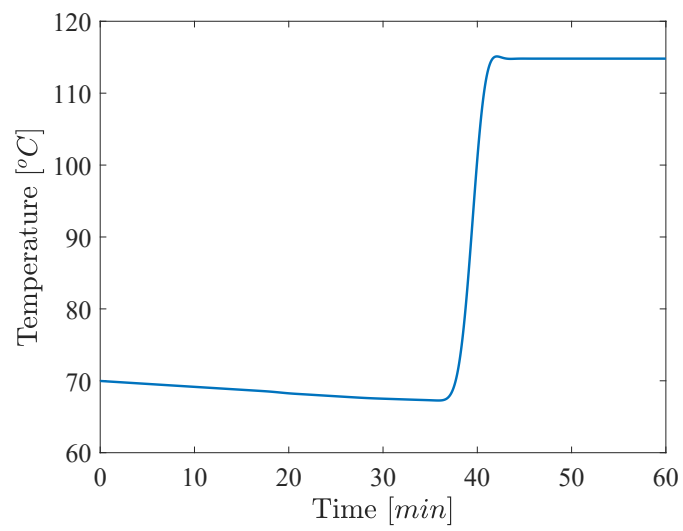


Figure 6.5: Temperature evolution of node 14, obtained inserting a *fictitious* node every 10 m and using a time step of 1 s.

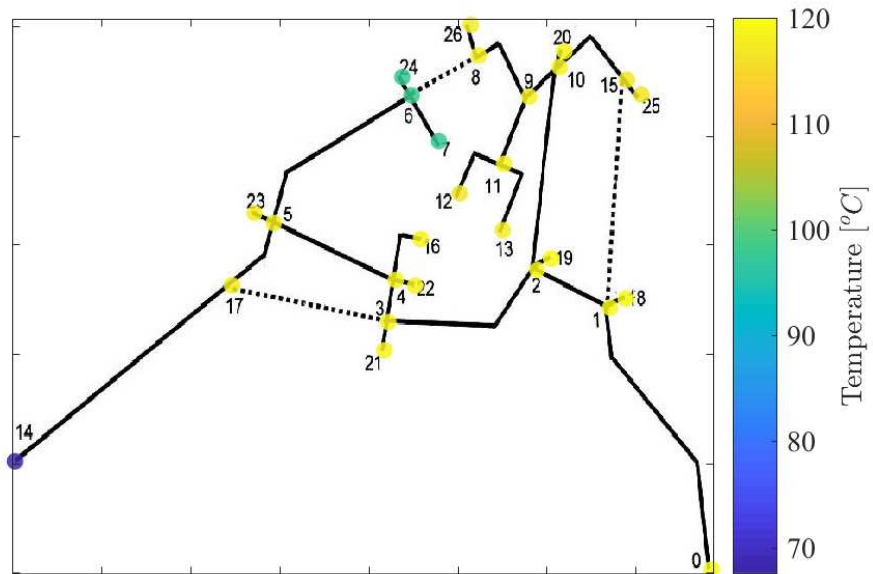


Figure 6.6: Temperature distribution at $t = 1800\text{ s}$ in the *real* nodes, obtained inserting a *fictitious* node every 5 m and using a time step of 1 s .

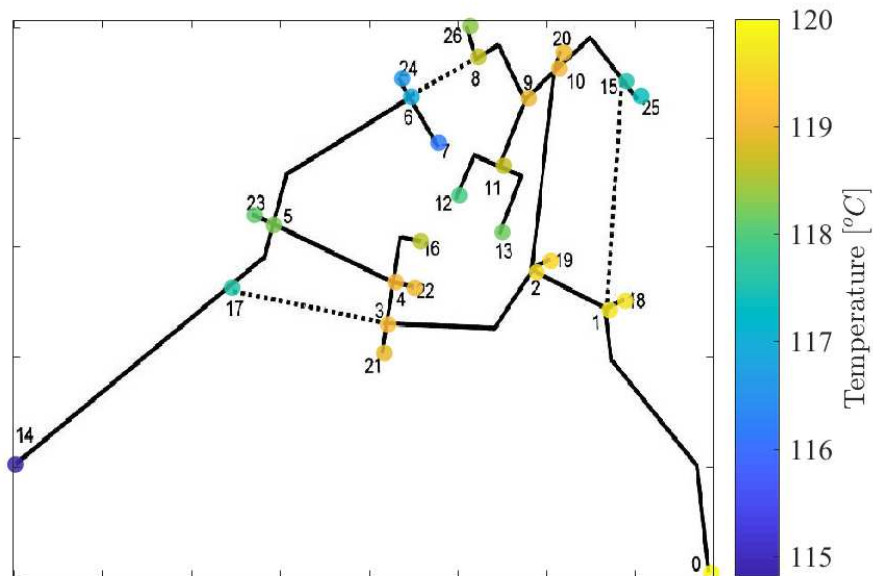


Figure 6.7: Temperature distribution at $t = 3600\text{ s}$ in the *real* nodes, obtained inserting a *fictitious* node every 5 m and using a time step of 1 s .

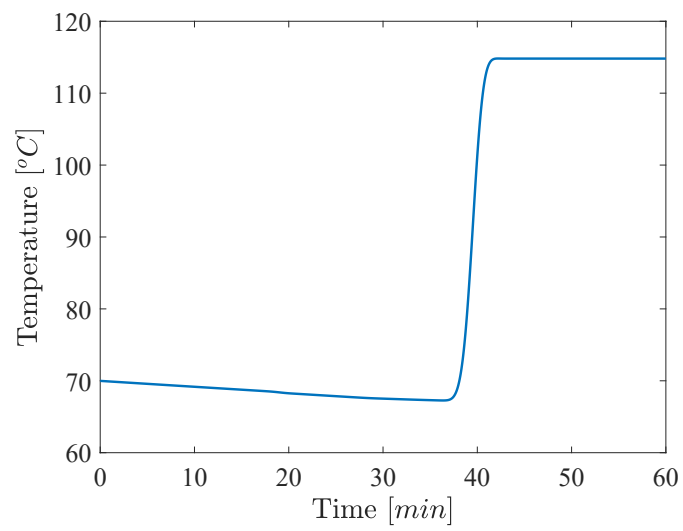


Figure 6.8: Temperature evolution of node 14, obtained inserting a *fictitious* node every 5 m and using a time step of 1 s.

Chapter 7

Conclusions

The scope of this work was to propose a numerical model able to describe in an accurate manner the thermal transients that occur in a district heating network. Indeed, predicting the temperature behaviour is essential to have a full control of the network, to reduce the temperature losses and to guarantee the thermal comfort of the users at a reasonably low cost, as explained in a brief introduction in Chapter 1. Therefore, a proper thermo-fluid dynamic model is needed. After having described the hydraulic part of the problem in Chapter 2, on the basis of what suggested by [8], the focus of the work passed on the thermal problem, solved by means of the finite volume method, developed in Chapter 3.

To solve the problem, an approximation of the values at the interfaces of the control volume has been needed. A description of why the Central Differencing Scheme cannot be applied in a case like district heating, strongly dominated by the advection contribution, has been carried out. Then, the Upwind Differencing Scheme (UDS) has been analysed, and it has been applied to a transient pure advection model problem in a pipe. In this way, the problem of the unphysical oscillatory behaviour given by Central Differencing Scheme has been solved. However, a new

problem emerged: the Upwind Differencing Scheme suffer from severe inaccuracies due to truncation error, that behaves in a similar manner to the diffusion term, introducing in the problem an artificial-numerical diffusivity.

Chapter 4 was dedicated on the analysis of some strategies to solve the issue of numerical diffusivity. The Quadratic Upstream Interpolation for Convective Kinematics (QUICK) introduced by [19] was found to be a good method to solve the problem.

Moreover, in Chapter 5, the effects of the use of an adaptive mesh methods to the transient pure advection model problem in a tube have been studied. Also this strategy has shown to produce satisfactory results.

Finally, Chapter 6 was dedicated to the development of a thermal model mainly based on QUICK, which uses UDS only in the nodes in which this method cannot be applied. The model proposed has been applied to a network taken from [11]. Thanks to this application it has been possible to show how it leads to adequate results.

Thanks to the good prospects of the model, as future work one can think to extend the application of the model presented to larger and real district heating networks. Moreover, another idea could be to apply moving meshes to a small network in order to investigate on the possible benefits that this kind of method can provide.

Bibliography

- [1] TAYLOR N.R., STIERHOFF K.L., *District heating handbook. A design guide*, International District Heating Association, Washington D. C. (1983).
- [2] REZAIIE B., ROSEN M. A., *District heating and cooling: Review of technology and potential enhancements*, Applied Energy 93 (2012) 2-10.
- [3] DOBOS L. ABONYI J., *Controller tuning of district heating networks using experiment design techniques*, Energy 36 (2011) 4633-4639.
- [4] DHC+ TECHNOLOGY PLATFORM, *District heating and cooling. A vision toward 2020-2030-2050*, March 2012.
- [5] FREDERIKSEN S., WERNER S., *District heating and cooling*, Lund Studentlitteratur, 2013.
- [6] WERNER S., *International review of district heating and cooling*, Energy 137 (2017) 617-631.
- [7] GIRAUD L., BAVIÈRE R., VALLÉE M., PAULUS C., *Presentation, validation and application of the DistrictHeating Modelica library*, Proceedings of the 11th International Modelica Conference, September 21-23, 2015, Versailles, France.
- [8] GUELPA E., SCIACOVELLI A., VERDA V., *Thermo-fluid dynamic model of complex district heating networks for the analysis of peak load*

- reductions in the thermal plants*, Proceedings of the ASME 2015.
- [9] GUELPA E., SCIACOVELLI A., VERDA V., *Thermofluid dynamic model of large district heating networks for the analysis of primary energy savings*, Energy (2017), <http://dx.doi.org/10.1016/j.energy.2017.07.177>.
- [10] SARTOR K., THOMAS D., DEWALLEF P., *A comparative study for simulating heat transport in large district heating networks*, International Journal of Heat and Technology 36 (2018) 301-308.
- [11] SCIACOVELLI A., VERDA V., BORCHIellini R., *Numerical design of thermal systems*, 2015, CLUT Editrice.
- [12] DEL HOYO ARCE I., HERRERO LÓPEZ S., LÓPEZ PEREZ S., RÄMÄ M., KLOBUT K., FEBRES J. A., *Models for fast modelling of district heating and cooling networks*, Renewable and Sustainable Energy Reviews 82 (2018) 1863-1873.
- [13] HARARY F., *Graph theory*, New Delhi: Narosa Publishing House, 1995.
- [14] MUNSON B. R., OKIISHI T. H., HUEBUSCH W. W., ROTHMAYER A. P., *Fundamentals of fluid mechanics*, John Wiley & Sons, 2006.
- [15] PATANKAR S.V., *Numerical heat transfer and fluid flow*, Series in computational methods in mechanics and thermal sciences, McGraw-Hill book company, 1980.
- [16] QUARTERONI A., SACCO R., SALERI F., *Numerical mathematics*, Springer, 2007.
- [17] VERSTEEG H. K., MALALASEKERA W., *An introduction to computational fluid dynamics: The finite volume method*, 2017, Pearson Education Limited.

- [18] GIRAUD L., PAULUS C., VALLÉE M., ROBIN J., *Dynamic modelling, experimental validation and simulation of a virtual district heating network*, Proceedings of ECOS 2015.
- [19] LEONARD B. P., *A stable and accurate convective modelling procedure based on quadratic upstream interpolation*, Computer Methods in Applied Mechanics and Engineering 19 (1979) 59-98.
- [20] HUANG W., RUSSELL R. D., *Adaptive moving mesh methods*, Applied Mathematical Sciences (2010), Springer New York.
- [21] SAUCEZ P., SOME L., VANDE WOUWER A., *Matlab implementation of a moving grid method based on the equidistribution principle*, Applied Mathematical and Computation 215 (2009), 1821-1829.
- [22] TANG H., TANG T., *Adaptive mesh methods for one- and two-dimensional hyperbolic conservation laws*, Society for Industrial and Applied Mathematics 41 (2003), 2, 487-515.
- [23] HUANG W., REN Y., RUSSELL R. D., *Moving mesh partial differential equations (MMPDEs) based on the equidistribution principle*, Society for Industrial and Applied Mathematics 31 (1994), 3, 709-730.